RADAR REFLECTIVITY TESTS AND ANALYSIS OF A LENTICULAR

PASSIVE COMMUNICATION SATELLITE

Prepared under Contract NAS 1-3114 Amendment No. 7
by Goodyear Aerospace Corporation
Akron, Ohio

for

NATIONAL AERONAUTICS & SPACE ADMINISTRATION

ABSTRACT

GER 12330

Monostatic and bistatic radar reflectivity tests were conducted on
gravity-gradient stabilized lenticular passive communications satellite
models. The overall effects of the lenticule, booms, canister, and
solar sails were determined. It was found that under the most adverse
conditions, the relatively large, metallic, gravity-gradient booms caused
some degradation of the return signal as compared to the lenticule alone.

Phase II of the test program consisted of reflectivity measurements to
determine the electrical discontinuity effects of representative seams
and materials.

Monostatic and bistatic radar reflectivity tests were conducted on five-foot diameter models of a lenticular satellite by Goodyear Aerospace Corporation (GAC) of Akron, Ohio. Rf tests were also conducted of several representative materials and gore seams to establish future design criteria. This work was conducted as Amendment No. 7 on Contract NAS 1-3114 from April through July 1965. The technical objective was to increase understanding of rf characteristics of the lenticular satellite through correlation of test results with theory and earlier test data, permitting recommendations to be made for future design, test, and system study programs.

The study results are presented in two separate reports for efficient use and dissemination of the information. This report includes a description of the test models, test equipment definition, test procedure review, summary of test results, correlation of theoretical and experimental data, and conclusions and recommendations for future studies. GER-12331* contains the test patterns taken on the program for use by specialists desiring a more detailed review of the rf phenomena.

The work was administered by the Applied Materials and Physics Division of LRC, with Mr. D. C. Grana from the Spacecraft Applications Section acting as Project Engineer. F.J. Stimler of the Space Systems and Analytics Division was the GAC Project Engineer. The work was conducted as a cooperative effort by personnel from several divisions within GAC for the various specialties listed below:

Design	H.W. Barrett
Model Fabrication	E. Duplaga
RF Test	W. D. Wheaton and G.M. Hazlip
RF Consultant	B. M. Miller and C. L. Gray
Planning	H. T. Stewart
Contract Administration	A. F. Tinker

*GER-12331, Radar Reflectivity Data on a Lenticular Passive Communication Satellite. Goodyear Aerospace Corporation, Akron, Ohio, September 1965.

CONTENTS

TABLES

ILLUSTRATIONS

ILLUSTRATIONS (Continued)

ILLUSTRATIONS (Continued)

Phase I and III Models and Requirements

TILT MECHANISM

SOLID MODEL WITH THIN BOOMS

SOLID MODEL WITH LARGE BOOMS

FIBERGLASS MODEL

- MODELS – 5-FT DIAM
- FREQUENCY ~ 9000 MC
- TILT ANGLE – 0 TO 40 DEG
- BISTATIC ANGLE – 0 TO 60 DEG
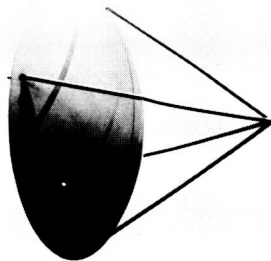
WIRE GRID/FOAM MODEL
POLAR CAP DESIGN
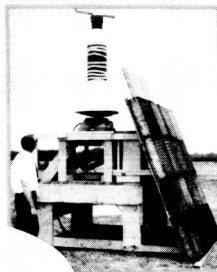
SETUP WITH REFERENCE CYLINDER

BISTATIC ANTENNA SETUP
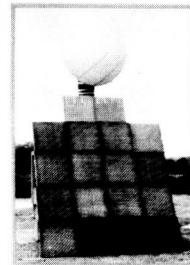
EQUATORIAL CAP DESIGN

GOODYEAR AEROSPACE

Phase II Models and Requirements
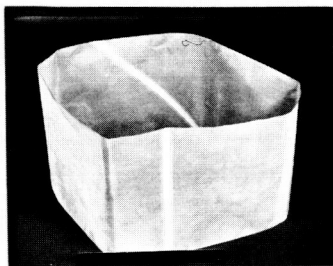
TYPICAL MODEL-VERTICAL AND 45-DEG SEAM
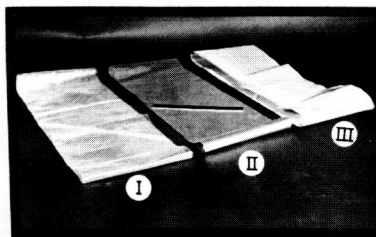
3 TYPES OF MATERIALS

I - 1.6-MIL PHOSPHOR BRONZE (24 X 24) 0.7-MIL PHOTOLYZABLE FILM (0.008 PSF)

II - 3-MIL ALUMINUM FOIL (0.036 PSF)

III - 5.5-MIL PHOSPHOR BRONZE (80 X 80) (0.16 PSF)
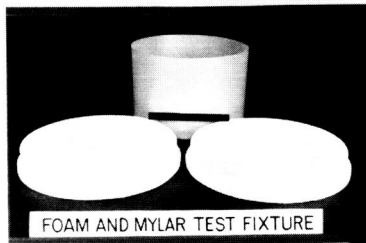
FOAM AND MYLAR TEST FIXTURE
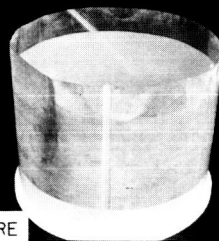
MODEL ON TEST FIXTURE

RF TEST SETUP

SEAM TYPES
(CONDUCTIVE AND NONCONDUCTIVE)
1/2-IN. GAP
BUTT
1/2-IN. LAP
3/4-IN. LAP

TEST CYLINDER -
12-IN HIGH X 20-IN DIAM.

GOODYEAR AEROSPACE

viii

RADAR REFLECTIVITY TESTS AND ANALYSIS OF A LENTICULAR
PASSIVE COMMUNICATION SATELLITE

SUMMARY

Goodyear Aerospace Corporation conducted monostatic and bistatic rf range tests and analyses with five-foot diameter solid surface and simulated inflated models of a lenticular passive communication satellite. The overall effects of the lens, booms, canister, and solar sail on the rf signal return were investigated. Tests were conducted at five X-band frequencies (8869, 8843.5, 8993.3, 9127.0, and 9263.1 Mc) and bistatic angles of 0°, 20°, 40°, and 60° for model tilt angles of 0°, 10°, 20°, 30°, and 40° for conditions with and without tetrapod booms attached to the lens. This resulted in over 200 test points. Since the bistatic test patterns of Phase I, in general, showed similar characteristics, it was considered advisable to eliminate the 80° bistatic test condition in favor of getting more test points of the Phase III models in various combinations. The rf effects of tetrapod booms of smaller diameter and a representative solar sail attached near the tetrapod apex were also investigated. The models and test setup, which are summarized graphically in the upper photograph of the frontispiece, are explained in detail in the body of the report. The tetrapod booms provide a configuration suitable for gravity-gradient stabilization; the solar sails are used for satellite station keeping.

Signal reflection from satellite booms agrees generally with theory. When designing lenticular satellites, allowances must be made for frequency-dependent changes in boom reflection cross-section and response angles. Model scaling of the booms considered availability of rf equipment and minimization of blockage of the lens rf signal. The cross-section ratio between the spherical portion of the lens and a boom of the full-size satellite was chosen at 2000 Mc where the ratio is 1.14 db. The full-size satellite has a lens diameter of 267 feet, a lens radius of curvature of 200 feet, a tetrapod boom diameter of 4 inches, and a boom length of 210 feet.

Rf measurements of the five-foot model lens were in agreement with earlier 20-inch model tests (ref. 1). Although the tetrapod booms cause some degradation of rf return of the lens near the central angles, the near rf return level of the satellite is relatively unchanged for the bistatic and tilt angles investigated. Present indications are that the rf effectiveness of the lenticular satellite from a communication systems viewpoint is not adversely affected by the boom; however, further studies in this area are recommended. Additional boom interference tests could be conducted using different model scaling techniques; however, other problems of very high frequency and tight model tolerances may result.

The edge diffraction phenomenon (ring effect), which represents the interference between the lenticular lens edge and spherical portion as reported earlier for the 20-inch model (ref. 1), was also experienced with the five-foot model. These monostatic and bistatic test results and the corresponding theory are unique. Correlation of the experimental data with known theory was not attempted in this program, but should be considered on future effort.

In the actual scale model, the intersection of the four booms of the tetrapod was slightly larger than the scale-model canister, so the overall blockage effects of the canister are reflected conservatively in the boom test results.

In Phase II of the program, rf tests were conducted at X-band on models of four types of seams (1/2-inch gap, butt, 1/2-inch lap, and 3/4-inch lap) with representative lens materials as summarized graphically in the frontispiece. The solid foil, close mesh, and loose mesh

materials were assembled into cylindrical models 20 inches in diameter and 12 inches high for monostatic rf range testing. An axial and 45° seam were put into each sample to improve detection of rf effects. Both nonconductive and conductive type seams were investigated for each condition, resulting in over 40 test points. In general, the 1/2-inch gap seam was easily distinguishable as an rf scintillation whether the seam was conductive or nonconductive. The lap seams gave the best rf return, with little difference between conductive or nonconductive seams. More significant results might have been possible had the rf polarization been parallel to the axial seam. The materials utilized in the seam test program showed similar rf characteristics for the test conditions investigated.

In Phase III of the program, two five-foot diameter foam lens models covered with conductive wire grid/photolyzable film material were tested on the rf range at frequencies of 8843 and 9263 Mc at bistatic angles of 0° and 20° and tilt angles of 0°, 10°, 20°, 30°, and 40°. Model A was of polar cap design; Model B, of equatorial cap design, was used to simulate an inflatable lenticular satellite (see upper photo in frontispiece). The material was 1.6-mil diameter phosphor bronze at 24 x 24 per inch with 0.7-mil photolyzable film cast to it. A 3/4-inch conductive lap seam was used to minimize rf scintillation. Tests were conducted with Models A and B in front of a reflecting surface for correlation with the solid model test data. In addition, combination models A/B and B/A were tested to determine significant rf effects of the grid material on the simulated inflated lenticular concept.

The rf return signal from the center of Models A and B, when tested with a similarly shaped reflecting-back lens surface, showed scintillation characteristics similar to those experienced with the fiberglass models that used conductive paint on the surface.

Test results indicated that there was no significant difference between the rf returns experienced with the polar cap lens panel design (Model A) and the equatorial cap lens panel design (Model B). The actual lens panel design will probably be predicated on material, structural, fabrication, and assembly limitations rather than rf requirements.

The rf test range was set up to give far-field scattering data by fulfilling the equation $R = 2D^2/\lambda$, where R = test range (ft), D = target aperture diameter (ft), and λ = operating wave length (ft). Therefore, a range approximately 470 feet in length was used for Phases I and III and a range 94 feet in length for Phase II. Some representative near-field rf signal data has been taken by other investigators and a comparison of the data may be enlightening.

Additional rf tests should be considered to determine the effect of boom included angle, tripod boom designs, and plane of polarization on boom interference of the lens rf return signal. It may be desirable to use smaller increments of tilt and phase angles in critical regions and more sophisticated test setups to get a better understanding of the interference phenomena encountered. Nonconductive booms should be considered for future satellite designs to minimize or eliminate rf interference with the lens signal.

Based on test results to date, inflatable satellites should be made with conductive, overlapping seams. Experience indicates that as a satellite rotates some phasing in rf scintillation due to the seams is possible. Additional tests of simple rotating models should be made for various polarization conditions. The models should be solid, rather than flexible, to eliminate fabrication tolerance effects.

Testing of inflated rather than simulated models may be the better approach to eliminate the foam filler and get the true effect of skin-wrinkling caused by packaging and actual seam construction. Clearly, new problems may arise in rf ground testing of inflated lenticular satellite models, and it may be desirable to go directly into a flight test experiment to obtain representative results of anticipated rf signal return and scintillation. A detailed and complete theoretical rf analysis of the lenticular satellite concept has not yet been made. Such an analysis might be helpful in developing the theoretical picture for use as a guide in future programs.

RF EFFECTS OF SIMULATED BOOMS, CANISTER,
AND SOLAR SAIL (PHASE I)

Introduction

Microwave scattering measurements were performed to determine the effects of the tetrapod and canister on the rf return from the lenticular concept and to more closely approximate the rf return from the full-size satellite.

Previous work on a 20-inch model showed interaction between the return from the spherical portion and return from the edge of the lens (ref. 1). Data from the tests resulted in establishment of a theoretical model that satisfactorily explained the rf return from the model (refs. 1 and 2). Since these lens tests were intended only to determine the interaction between the returns from the spherical portion and the edge, no correlation between the return from the 20-inch model and the return from the full-size satellite was expected. (See fig. 1.)

A basic requirement of the lenticular-type satellite is that it be provided with some type of stabilization. A tetrapod of support booms on each side of the lenticular surface has been determined as necessary to achieve satisfactory gravity-gradient stabilization (see fig. 2). Since booms and canister hardware are needed on both sides, one set must necessarily be in the rf field, and will cause perturbations of the reflected wave. This program was initiated to determine these perturbations.

At the start of the program, very limited theoretical and experimental data was available for the lenticular configuration under consideration. Also, there was some concern over correlation of theory with near- or far-field test data. Therefore, this report presents some basic monostatic and bistatic far-field data for ready correlation and guidance when considering future theoretical and experimental programs in the critical areas of interest.

Model Scaling Considerations

General. - The lenticular satellite concept attempts to obtain radar performance comparable to that of a very much larger sphere. The lenticular shape, which is advantageous because of a much larger lenticular using gravity-gradient stabilization, could be orbited within the same weight requirement as a given sphere. Pertinent dimensions of a full-scale satellite are given in figure 2.

Actual frequency scaling of the satellite was not practical because of its large size and the intended 2 to 10 kmc range of operating frequencies. A proper scaling of the 267-foot (200-foot radius of curvature) satellite to a manageable size would result in a test frequency of approximately 185 Gc. Hence, it was necessary to use another scaling scheme for practical tests.

Spherical portion. - The 20-inch model tests indicated that the average monostatic return (excluding interference effects) closely approximates the return expected from a full sphere of the same radius of curvature. The 20-inch model had a diameter to radius of curvature ratio (D/R) of 1.25. The model diameter was approximately 17 wave lengths at the X-band test frequency, which placed it out of the resonant region.

The model chosen for this program had the same diameter to radius of curvature ratio (D/R = 1.25) as the 20-inch model, and had a diameter of 5 feet (scale factor = 0.0187), or approximately 50 wave lengths at X-band. At this size, variations in the return due to resonance effects are small (less than 0.2 db) and should provide further verification that the return will approximate that of a full sphere.

Since the X-band test frequencies place this size model well outside the resonant region where the return from the spherical portion is essentially constant, the fact that a true scaling frequency was not used should not affect relative radar cross section magnitudes. The theoretical magnitudes of the full-size satellite and the five-foot model are 12.6×10^4 sq ft and 50.3 sq ft, respectively.

Tetrapod booms. - The theoretical cross section of a single boom for the full-size satellite is 9.67×10^4 sq ft, assuming that the rf is at normal incidence, polarized parallel to the boom, and that it has the following dimensions:

Boom length = 210 ft
Boom radius = 0.171 ft
Frequency   = 2000 Mc

This is the maximum value of the radar cross section. For arbitrary angles of incidence and polarization, the return is given by

$$\sigma = \frac{\pi L^2 \sin^2 \theta \left[\dfrac{\sin\left(\dfrac{2\pi L}{\lambda} \cos \theta\right)}{\dfrac{2\pi L}{\lambda} \cos \theta} \right]^2}{(\pi/2)^2 + \left(\ln \dfrac{\lambda}{1.78 \, \pi a \sin \theta} \right)^2} \cos^4 \phi \qquad (1)$$

where

L = length of boom

a = radius of boom

θ = angle between boom axis and direction of propagation of rf

ϕ = angle between boom axis and rf polarization

The equation indicates rapid decline of radar cross section for small changes in angle of incidence. Since the booms are inclined 49.4° from the satellite axis, the return due to the tetrapod is down considerably from usable satellite look angles, as shown in the sketch on the following page.

Since the radar cross sections of spheres (ref. 3) and cylinders (ref. 4) are different functions of their dimensions, their relative returns are not of the same proportionality when scaled by the same dimensional factor. Since the cross section of the full-size spherical part is 12.6×10^4 sq ft and the cross section of a full-size boom is 9.67×10^4 sq ft, a model should present the same ratio (1.14 db) of spherical cross section to boom cross section. This would require the scale-model boom to have a maximum cross section of 38.4 sq ft. The length of the five-foot model boom, physically scaled from the full-size satellite, is 3.93 feet. For this boom length to present the required cross section, a 0.0407-foot radius is required.

84°

Peak boom return

49.4° 81.2°

θ

Incident rf energy
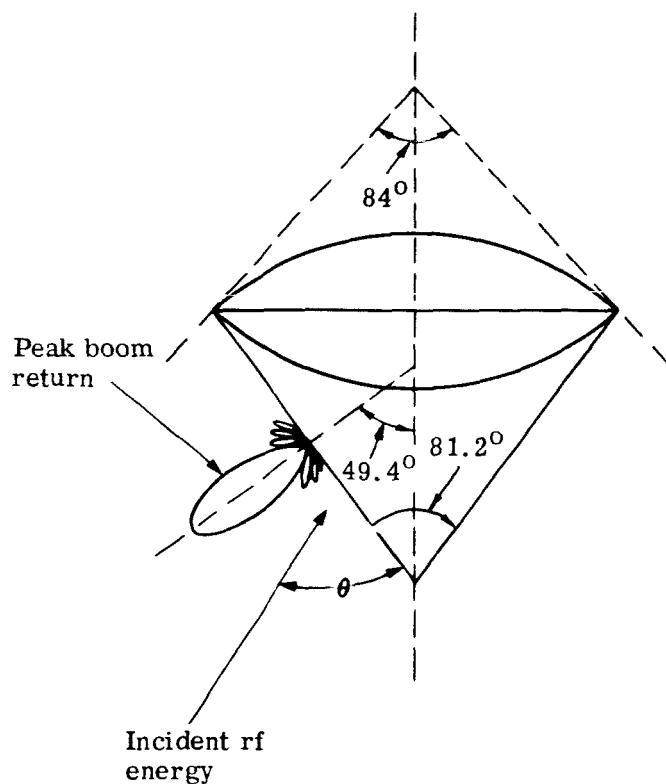
Canister. - In order to obtain consistent rf results, the same scaling technique should be used for the canister. The canister is essentially a spherical container 4.16 feet in diameter. Since both the canister and satellite are spherical, a physical scaling is equivalent to cross-section scaling. The canister for the five-foot model will be 1.05 inches in diameter. Its cross section is then 6.01×10^{-3} sq ft, or approximately 39 db below the spherical portion.

In the actual scale model the intersection of the four booms of the tetrapod is slightly larger than the scale-model canister.

One precaution must be observed in regard to the canister. Should the canister cause excessive blockage of energy that would normally strike the lens, serious degradation of efficiency could result. This effect can most readily be seen by evaluating the blockage of the first Fresnel zone.

The Cornu spiral is a helpful device for illustrating this point (see sketch on the following page). Dividing the first zone into subzones, we find that the amplitude vectors from the subzones extend from A to B, as shown in sketch (a), giving a resultant return $E_1 = AB$ for the first zone only. The second zone alone similarly gives those between B and C with a resultant $E_2 = BC$. For these first two Fresnel zones, the total contribution is then $E_1 + E_2 = E = AC$. Since the amplitudes E_n decrease rapidly for $n \to \infty$, the resultant of all zones

(a)   (b)
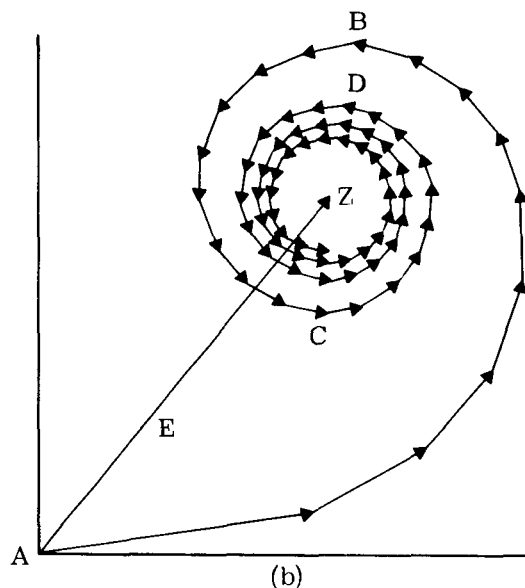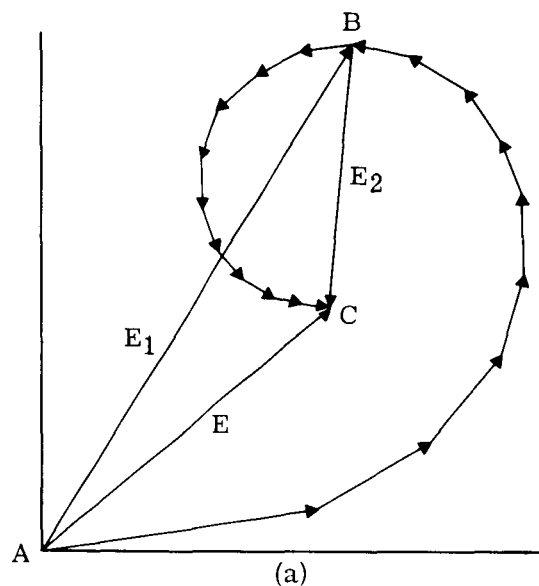
is $E = AZ$, as shown in sketch (b) above. Thus it can be seen that after the first few zones, contributions from the remaining zones are vanishingly small. (This also illustrates the basic idea of the lenticular concept.) The five-foot model includes approximately 16 Fresnel zones.

The five-foot scale model has a first Fresnel zone diameter, at the test frequency, of approximately 10.9 inches, while the canister diameter is of the order of 1.0 inch. Hence the canister blocks only a small portion of the first Fresnel zone (3.5 sq in. of 373 sq in., or less than one percent), and no degradation should result.
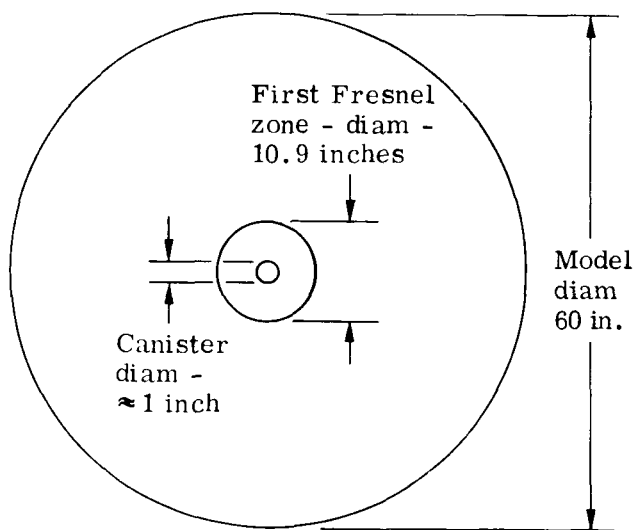
Edge effects. - Tests of the 20-inch model indicated that a definite interference pattern exists due to edge diffraction return. This is caused by a phase difference between the return from the spherical portion of the satellite and the return from the edge discontinuity. It has been shown that the lenticular configuration may be considered as two scatterers, the primary one being a sphere representing the spherical portion of the satellite, and the secondary one a ring representing the edge of the spherical section. Since the ring has significant return only in the "on axis" direction, interference will be seen only in the "on axis" aspect angle of the satellite and for small increments about that angle.

The same effects were expected and were found in the five-foot model. However, because of the increased diameter of the model the interference has a more rapid variation with aspect angle.

Scale model. - A practical scale model for testing at five X-band frequencies was designed under the considerations discussed above. The lens section of spherical caps was physically scaled from the satellite by a ratio of 0.0187. The booms were physically scaled in length by the same ratio, but were scaled in diameter by radar cross section (RCS). The ratio of normal incidence, parallel polarization boom RCS to lens RCS is 0.769 (1.14 db), a constant of the proposed satellite and the scale model. Thus any interactions between the booms and the lens will be of the same magnitude in the scale model measurements as in the full-size satellite. Pertinent dimensions of the scale model and the full-scale satellite are compared in table I.

Model Fabrication

The five-foot diameter test model shown in figure 3 was fabricated using an epoxy preimpregnated fiberglass cloth in an available mold. The lenticular-shaped plastic model was formed by bonding together two spherical shells having a diameter of five feet and a curvature radius of 48 inches. Each shell, oven cured applying the vacuum bag technique, was approximately 0.060-inch thick with an additional 0.030-inch thickness around the periphery forming a two-inch band of reinforcement. Four 3 x 3 inch wooden wedges were equally spaced and bonded around the inside edge of each shell for the installation of the tetrapod booms (see fig. 4). An additional integral 0.040-inch thick laminate backup, tapered to a diameter of 20 to 22 inches, was bonded on the inside apex of the bottom shell for mounting the model on the test fixture for reflectivity tests. The model was sprayed with a silver, metallic-loaded, polyester resin to provide an rf-reflective surface. Figure 5 shows the sprayed model with and without the booms attached. Materials used for fabrication of the model are listed in table II. Formulations used are listed in table III.

Reflectivity Tests

General. - Since it is not possible to predict theoretically the resultant of all interactions on the radar return from the lenticular satellite, a large number of patterns of the five-foot model radar reflectivity were measured.

Test program. - Monostatic and three bistatic measurements of the five-foot model satellite reflectivity were made at five X-band frequencies (see table IV). At each angle and frequency five elevation or tilt angle cuts were measured, both with and without the tetrapod booms attached.

The five test frequencies were chosen as representative points on the curve plotting interference between the specular return and the edge diffraction or ring return. Assuming the edge diffraction return has a 180° phase shift relative to the specular return (ref. 2), then the return signals are in phase when $d = (\lambda/4)(2n-1)$, where d is the half thickness of the lenticular, λ is the operating wave length, and $n = 1, 2, 3 \ldots \ldots$. Dimension d of the model is 10.53 inches.

Solving for λ, the result is $\lambda = 4d/2n-1$ (in-phase condition).

For the out-of-phase or null condition, the corresponding result is $d = n\lambda/2$, or $\lambda = 2d/n$. Figure 6 is a plot of these conditions and shows the model test frequencies.

The 20-inch model measurements were all made monostatically; hence, it was highly desirable to obtain bistatic data from the five-foot model. Measurements were completed at three bistatic angles, 20°, 40°, and 60°, in addition to monostatic. Since all patterns were cut through the azimuth plane, it was necessary to tilt the model in elevation to obtain off-axis data. Patterns were measured with five tilt angles, 0°, 10°, 20°, 30°, and 40°. Figure 7 shows the position of the model for the various tilts.

Because of the marked effects of the scaled tetrapod booms on the model rf return, a second boom set of smaller diameter was measured at 9263 Mc at a bistatic angle of 20°. These small booms were copper wires of 0.064 inch diameter. A foam column 1-1/2 inches in diameter by 29 inches long was used to tension the wires (see fig. 8).

The rf effect of a solar sail was also investigated. A scale model sail 12 inches high was inserted vertically at the apex of the booms and the return measured for the 60° bistatic angle and 9263 Mc frequency condition.

Test range. - A ground range 470 feet in length was used to make all reflectivity measurements. The range length was chosen to satisfy the usual $\lambda/16$ phase criterion, $R = 2D^2/\lambda$, where D is the diameter of the model (five feet) and λ is the operating wave length. The amplitude variation over the region occupied by the model was held to less than ±0.5 db as verified by field probes.

The transmitter was a phase-locked reflex klystron with 27 dbm of cw power. The phase lock is used as a convenient way of achieving frequency stability. For the monostatic measurements only, part of this power was coupled off to a background canceling network. Figure 9 shows the monostatic waveguide setup, and figure 10 shows the bistatic arrangement. Because of the wide separation at the bistatic angles, use of a canceling network was not possible. Horizontally polarized 42-inch and 51-inch diameter parabolas were used as transmitting and receiving antennas, respectively. Referenced to the transmitter beam, the 20° and 40° bistatic measurements were made with the receiving antenna to the right, and the 60° bistatic patterns were made with the receiving antenna to the left.

The model and reference cylinder support was a 1.5 lb/ft³ polystyrene foam post, 5.5 feet high and 11.7 inches in diameter. A single-axis gimbal system at the top of the post allowed tilt motion of the model. For reference cylinder measurements, the model and gimbal system were removed and replaced by a foam cap designed to hold the cylinder. The support post was attached to an azimuth rotation sitting on a platform stand. An absorber wall of CV-6 absorber, 8 x 8 feet, was used to reduce the return of the rotator and stand. (See fig. 11.)

Test procedure. - The procedure used to measure the satellite radar return is described below.

(1) The background noise pattern was measured with foam support post in place.

(2) The return of 30-inch and 12-inch long reference cylinders was measured.

(3) Background noise level was remeasured to ensure system stability.

(4) Return from scale model satellite, either with or without booms, was measured at all five tilt angles. When the model was measured with booms, the booms were oriented parallel and perpendicular to the polarization.

(5) Background level was remeasured.

8

(6)   Return from large reference cylinder was remeasured to assure overall system stability during model measurement.

Since this procedure was followed for all reflectivity patterns measured, a set of patterns is needed to comprise any given measurement.   The background noise level was at least 20 db below the peak model return level, except in a few isolated cases over small angular regions.   All patterns were recorded with the model rotating in the clockwise direction, looking down on the mount from above.   The pattern recording begins on the right-hand side of the paper under the title block.   No attempt was made to reference the pattern zero in any fixed direction.

Reference cylinders. - A series of four cylinders were fabricated to serve as calibration references, both for range check-outs and as a standard return level.   The cylinders were 3.49-inch diameter, seamless extruded aluminum tubing cut to length.   The cylinder lengths, cross section, and relative levels are given in table V.   The values of absolute cross section will decrease for increasing bistatic angle.   (A paper presenting the techniques for computing these values is in the process of publication by Goodyear Aerospace Corporation.)

Results and data analysis. - The test program is summarized in table IV, which gives the reference number for each test run.   General characteristics of each pattern have been reviewed below to aid in data evaluation.   The return levels given are the mean return from the model over the angles where the return is approximately flat and variations are small.   In regions where the variations in the return are not small, mean levels have no useful meaning.   The levels are referenced to the 30-inch long reference cylinder in each case. Accuracy of the mean levels is approximately ±0.5 db.

In figures 12, 13, 14, 15, and 16, the mean relative cross section of the model both with and without the tetrapod booms has been plotted against tilt angle for each bistatic angle and frequency.   The reference cross section in each case is the cross section of the 30-inch long reference cylinder at that frequency.   These three-dimensional plots accentuate general trends and questionable areas.

Monostatic condition:

(1)   Without tetrapod booms.   The mean levels are near the reference level for the first four tilt angles (0°, 10°, 20°, and 30°), dropping off 6 to 8 db for the 40° tilt position.   One anomoly in the return, which occurs in both monostatic and bistatic data, is that the right side of the pattern is down approximately 0.5 db.   This anomoly is evident both with and without booms.   A possible cause may be an asymmetry in the model, since all patterns were measured identically.   Of the measured returns, a definite interaction between the spectral return and the edge diffraction return was noted only at 9127 Mc, both with and without the booms.   Figure 17 is a repeat set of data for the monostatic condition model without booms, at 9127 Mc frequency. It shows clearly that data variation within the range of 0.5 db can be expected with tilt angles of less than 40 degrees.

(2)   With tetrapod booms.   The level at the 0° tilt position is down 2 to 4 db from the reference, but comes up to approximately -1 db for the 10°, 20°, and 30° tilts.   The 10° tilt pattern has a broad deep hollow in the center for three frequencies - 8669, 8993, 9263 Mc.   The return drops to -6 to -10 db for the 40° tilt.

20° bistatic condition:

(1)   Without tetrapod booms.   Generally the return is down about 1 db, with maximum ripple amplitude around 5 db for the 0°, 10°, 20°, and 30° tilts.   At 40°

tilt the level is down 2 to 8 db, except at 9127 Mc where a unique type of re-
turn occurred. The pattern here is very round and smooth with coma lobes.
The peak level is 1 db above the reference cylinder level. The spectral-edge
return interaction is noticeable only at 9263 Mc.

(2) With tetrapod booms. At 0° tilt the levels over the five frequencies are 1 to 5
db down. At the other tilt angles, the level is near the reference, except 40°
which is 1 to 9 db down. The right side of the patterns, both with and without
booms, is approximately 0.5 db low.

(3) With small tetrapod booms. The return from the model with the small booms
was very similar to the return with the scale model booms, as can be seen in
figure 18. As would be expected, the boom interactions were reduced. The
normal incidence, parallel polarization return from the small booms is theo-
retically 11.4 db less than the return from the scale model booms. The small
booms were tested to determine if any gross interference effects could be de-
tected resulting from boom blockage; however, the size had no scaling logic.

40° bistatic condition:

(1) Without tetrapod booms. The mean level for 0°, 10°, 20°, and 30° tilts is
about 1 db below the reference level, except at 8669 Mc where it is about
equal to the reference level. The return at 40° tilt is -6 to -10 db. At 8843,
8993, and 9263 Mc a broad dip appears at 30° tilt, which is of the order of 3
db deep. The interaction between spectral and edge return turns up at 8843
and 9127 Mc in its strongest appearance, where the peak-to-null amplitude
is 12 db. Also, the right pattern side is 0.5 to 1 db lower than the left.

(2) With tetrapod booms. The zero degree tilts are 3 to 5 db down from the
reference with the phasing interaction at 8843 and 9127 Mc (null-to-peak
amplitude is 10 db). The 10°, 20°, and 30° are up to 3 db below the refer-
ence, except for the 8669 Mc 10° and 30° tilts which are up 2 db and 1 db,
respectively. Broad center dips occur at 10° tilt at 8843 and 9263 Mc, at
20° tilt at 8993 Mc, and at 30° tilt at 8843, 8993, and 9263 Mc.

60° bistatic condition:

(1) Without tetrapod booms. All five frequencies have interaction phasing at the
0° tilt position. The mean levels for 0°, 10°, and 20° tilts are approximately
equal to the reference level. The level for the 30° tilt is 0.5 to 1.5 db above
reference level. The 40° tilt pattern levels are 6 to 9 db down.

(2) With tetrapod booms. The 0° tilt level is down approximately 3 db with strong
center phasing. At 10° tilt the mean level varies from -2 db to +1 db with
broad center dips, except at 8993 Mc where the edges are low. The 20° tilt
levels are at about reference level, with three frequencies showing narrow
dips at the center (8669, 8843, and 9127 Mc). The 30° tilt levels are up 0.5
to 1 db with narrow dips at 8993 and 9127 Mc. The 40° tilt patterns are 6 to
8 db down with narrow center dips at 8669 and 9127 Mc.

(3) With tetrapod booms and solar sail. A triangular piece of aluminum approxi-
mately 12 inches high was placed between two diametrically opposite tetrapod
booms, beginning at the apex to simulate the full-scale solar sail condition.
The solar sail was placed in the vertical plane during tests to get the maximum
effect on rf return. The 0° tilt return has a rather unique appearance in the
head-on direction as shown in figure 19. The solar sail appears to interact
strongly with the edge diffraction return. Outside of the interaction region,
the mean level is about 2 db below the reference level. The 10° and 30° tilt
angles average 1 db above reference level, with both showing broad center dips.
The 20° tilt return level is near reference level and 40° tilt is about 8 db down.

10

Summary of test results. -
The rf return from the five-foot
model is very comparable to the re-
turn from the 20-inch model. The
return is fairly constant over an
angle of about 65° for the 0° and
10° tilts and about 5° less for 20°
tilt. For 30° tilt the flat region
has narrowed to approximately
40°. Expectedly, the return at
40° tilt is down considerably.
The mean radar cross section for
the model without the tetrapod
booms for angles, where it remains
approximately constant, is 80 to 100
percent of the reference cylinder
cross section, or 40 to 54 sq ft.

Receive | Transmit

Far angle spike

Receive | Transmit

Near angle spike
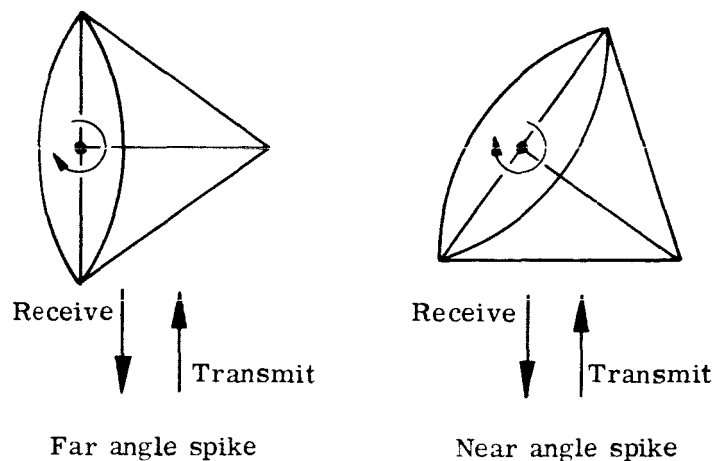
The model return with the tetrapod booms in place shows some phasing. For the 0°
tilt positions boom interaction is quite strong, as the mean cross section of the model is re-
duced by 3 to 5 db. Mean return levels for the 10° tilt positions vary ±1 db from the mean
level without booms, depending on frequency and bistatic angle. For 20° and 30° tilts the
cross section remains fairly constant at about 52 sq ft. The cross section varies erratically
for the 40° tilt positions, and is 2 to 10 db down. In all patterns with the tetrapod booms, it
will be noticed that a sharp spike is located at either side of the specular return of approxi-
mately the same amplitude. In some cases a second spike will be seen at near ±90° (if the
patterns cover that broad an angular range). These pairs of spikes are caused by broadside
return from the horizontal and vertical pairs of booms; the far angle pair by the vertical and
the near angle pair by the horizontal booms. This is easily seen from the above sketch for
the monostatic case.

Conclusions and Recommendations

The model scaling technique used appears to be the best method for scaling and gives
valid results. However, it should be pointed out that the particular case chosen for scaling
the satellite is a best-case example.

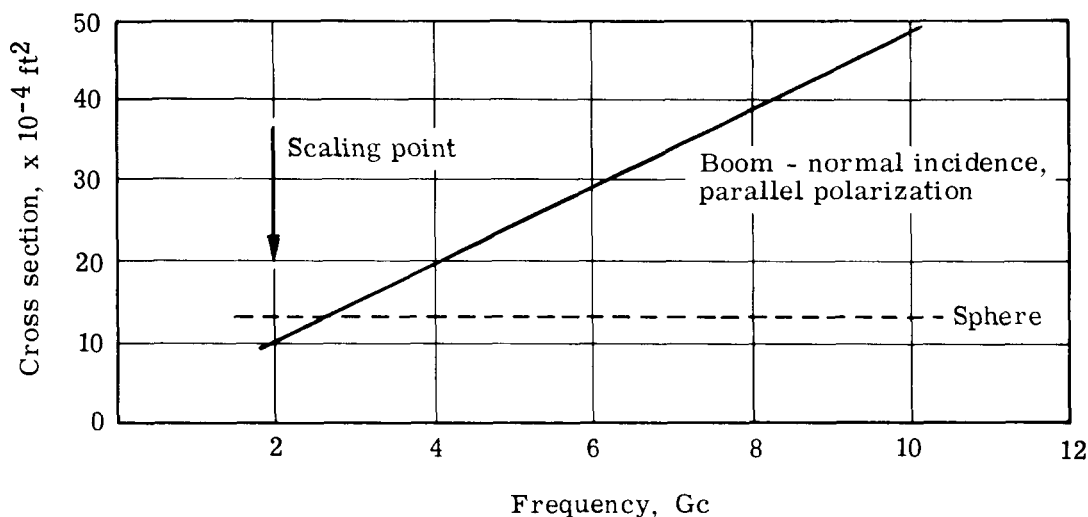The radar cross section of a cylindrical boom (ref. 5) is given by

$$\sigma_c = \frac{2\pi}{\lambda} r \ell^2$$

for normal incidence and parallel polarization. Therefore, the cross section of a boom is
proportional to $1/\lambda$. The radar cross section of a sphere (ref. 5), on the other hand, is
given by

$$\sigma_s = \pi r^2,$$

which is independent of frequency. For purposes of building the scale-model satellite, the
cross-section ratio between the spherical portion and a boom of the full-size satellite was
chosen at 2000 Mc, where the ratio is 1.14 db.

Because of the $1/\lambda$ dependence of the boom radar cross section, it was desirable to conduct the model tests at the highest practical frequency. X-band was chosen, since components and a suitable power source were readily available. Also, model tolerances at higher frequencies would become a severe problem. With the test frequency band fixed, an operating frequency of the satellite for scaling needed to be chosen. Basically, the choice was reduced to keeping the scale model booms to a reasonable diameter to avoid excessive blockage of the sperical portion of the model. Even under these restrictions the booms were nearly an inch in diameter. Within these bounds, the 2000 Mc frequency was picked as the scaling point.

The graph above shows the radar cross section of a full-scale boom as a function of frequency for normal incidence and parallel polarization.

The measured radar return patterns of the five-foot scale model with the booms indicate some degradation of return relative to the model without booms. Although the average return level is not too adversely affected, the return does fluctuate rather rapidly with angle with peak-to-peak amplitudes of 3 to 5 db. However, it should be remembered that the data was deliberately measured for the worst case - one pair of booms directly in the plane of polarization. This, no doubt, accounts for the lower return at 0° tilt angles. This problem should be studied from a communication systems viewpoint to evaluate its overall effects. Should this be too detrimental to system performance, a nonconducting type boom should be considered; or possibly a boom of different shape would improve performance. Another alternative would be to reduce the boom diameter, although the diameter is probably already minimum for its mechanical loading.

If further boom investigations are made, the radar cross-section scaling technique should be used, but at a higher satellite frequency (see graph above). This will necessitate scale-model testing at a higher frequency, since otherwise the boom diameter would be appreciable and would cause an unrealistic result because a considerable part of the lens would be blocked by the booms.

The interference effects between the edge and spherical portion of the lens in the return were found in the measurements of the five-foot model. No attempts were made to correlate the five-foot model data with the theory developed from the 20-inch model data.

A considerable amount of good basic data for the solid reflector type lenticular model has been obtained. This data was measured for both monostatic and bistatic conditions up to 60°.

Recommendations for further tests or study would include possible reduction of the boom-lens interactions by changing boom configuration; e.g., changing from a tetrapod to a tripod or changing the included angle between the booms. Data should also be acquired for the case where the boom is out of the plane of polarization.

## ELECTRICAL DISCONTINUITY EFFECTS OF REPRESENTATIVE SEAMS AND MATERIALS (PHASE II)

Introduction

Significant amplitude variations have been observed in the scattering patterns of wire grid spheres (refs. 6 and 7). (These results have also been found in the Echo type satellite, as discussed in reference 8.) These spheres comprised geodesic segments of grid material, such that continuity was not maintained from one segment to the next. (See fig. 20.) Extensive analysis indicated that this lack of continuity was a major contributor to the variations in amplitude of the scattered energy. As a result of these observations, the empirical seam study herein described was proposed and subsequently conducted.

Reflectivity investigations were carried out in this phase on three different types of materials to determine mesh effects. Seams were evaluated by measurements on four types of commonly used seams (both conductive and nonconductive). Also investigated was the effect of polarization angle with respect to the wire in the grid materials.

Model Definition and Fabrication

Material samples forming cylinders 12 inches high and 20 inches in diameter were fabricated from three representative satellite materials, which are defined in table VI. Each sample had a vertical and 45-degree seam at opposite sides (see sketch). The material samples constructed and tested during this program are shown in table VII. Table VIII defines the seam types under consideration for both the conductive and nonconductive cases. Figure 21 shows the positions of the seams with relation to the wire grids. The medium-mesh material was included in the program to get additional test points in key areas. The continuous reflecting surface had only a vertical seam so that rf data could be obtained as a reference on an uninterrupted surface for the three materials.
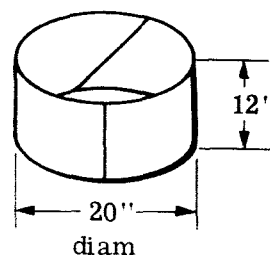
The material samples were held in place on a cylinder with foam ends, using a Mylar sleeve of 14-mil thickness for ease in model changing and uniform stretching of the seam samples. Figure 22 shows how the Mylar cylinder was formed over a wooden tool and also how the foam caps/Mylar cylinder unit is assembled.

Reflectivity Tests

Test program. - Monostatic measurements of the test samples were performed at a single X-band frequency. Table IX outlines the test parameters and identifies each test according to the number assigned to the data pattern.

Test range. - The measurements were made on a 94-foot ground range, which satisfies the far-field criterion for the antennas and target. Amplitude variations over the target aperture were ±0.3 db, as measured by a field probe.

The radar plumbing used was identical to that for Phase I (see fig. 9). The antennas were horizontally polarized horns with 10 x 12 inch apertures. The range was operated at 8843 Mc for all seam study measurements. Figure 23 shows the range with the absorber wall used in front of the mount removed.

Test procedure. - The sample to be tested was mounted on a heavy Mylar backing cylinder and two urethane foam end caps were inserted to rigidize the cylinder. A small absorber cylinder (Eccosorb AN-73 backed by aluminum) was placed inside the sample to minimize the effects of energy penetrating the sample. The samples were then placed on a polystyrene foam support column (see fig. 24) and 360° azimuth patterns recorded.

Each series (one orientation of the material with the four types of seams) of tests was measured in conjunction with a primary reference cylinder (Model No. XIII) of solid aluminum foil with one vertical overlap seam. Also, for each type of material there was a secondary reference sample of that material with a single vertical overlap seam.

The measurements were performed in the following manner:

(1) Extraneous background return was reduced to a minimum and recorded.

(2) The primary reference cylinder was placed on the mount and its return recorded.

(3) The secondary reference sample was mounted and its return recorded.

(4) Each of the four samples with different types of seams was mounted and each one's return was recorded.

(5) The return from the primary reference was re-recorded.

(6) The background return was rechecked and recorded to ensure that no changes had been incurred.

On each test sample pattern the vertical seam position was clearly marked.

Data analysis. - Detailed analysis of the test data (see patterns in GER 12331*) was limited to the region ±18° each side of the vertical seam, since the scattering from the 45° seams was slight and so inconsistent that no useful information could be deduced. The seam effects appear in the return as amplitude oscillations generally symmetric about the seam. Difficulty was encountered in obtaining valid seam effect data because the effect is small, and other small perturbations such as material wrinkling easily mask the seam effect.

---

*GER-12331, Radar Reflectivity Data on a Lenticular Passive Communication Satellite: Goodyear Aerospace Corporation, Akron, Ohio, September 1965.

In the bar charts shown in figures 25 through 29, the peak-to-peak oscillation amplitude in the 36° seam region has been plotted against the four types of seams with conducting and nonconducting adhesives. In no case did the mean radar cross section of the test sample vary more than 0.5 db from the mean radar cross section of the primary reference.

Conclusions

As might be expected, the gap joint gave the poorest results and making the joint conductive only gives minor improvement over the nonconductive gap joint. Performance is improved by butting the joint, but experience on other programs has shown that the butt often becomes a gap. Metalizing the butt joint generally makes it comparable to the lap joint.

Best results are obtained with overlapped type joints. Both a 1/2-inch and a 3/4-inch overlap seam were tested and no significant difference was apparent. Again, making the joint conductive made little difference.

The samples were all tested with seam vertical and horizontal rf polarization, since it was theorized that the two pieces of material were acting as separate scatterers. It is recommended in any further work that samples also be tested with the polarization parallel to the seam. Considerable scattering may be caused by the seam itself.

RF TESTS OF A SIMULATED INFLATED LENTICULAR SATELLITE (PHASE III)

Introduction

Investigations of the grid-sphere program (refs. 6 and 7) have indicated an interaction of energy reflected from the front of the sphere with energy that is able to penetrate the sphere and is reflected from the back surface. Because of the similarity of the grid sphere and the lenticular type materials, it was reasonable to expect a similar effect with the lenticular satellite. Phase III of this program was designed to test a simulated inflatable model to determine if this effect does arise and what the result might be on the radar reflectivity of the lenticular satellite.

Also, an investigation of two methods of fabricating the satellite was made in this phase of the program. Obviously, because of the size of the satellite, it is necessary to join together many sheets of the grid material. Several choices of individual panel shapes are possible, each resulting in a different geometric configuration of the seams. Two such choices were fabricated and evaluated.

Model Definition and Fabrication

Two five-foot diameter models were fabricated of a rigid polyurethane foam of 2 lb/ cu ft density covered with wire grid material to simulate (from an rf standpoint) an inflatable

lenticular satellite, as shown in figure 30. Each half was considered a complete rf model. Model A utilized a polar gore pattern and Model B an equatorial gore pattern over the convex surface, as shown in figure 31. Conductive-type seams of 3/4-inch overlap were recommended and used as a result of the Phase II studies.

Detailed information about the materials utilized for this phase can be found in tables II and III.

Model Test Assemblies

To adequately separate the rf penetration effect it was necessary to test each of the two panel configurations with the same "reference back half" of the model and also with one panel configuration backed up by the other. To allow maximum flexibility of a minimum number of models, the Phase I solid fiberglass model was separated into front and back halves and the back half (Model C) used as the "reference back half" for this phase. The two panel configurations, hereafter called Models A and B, were made by placing the lenticular grid material over a very low-density foam. Model A was made of pie-shaped gores around a circular cap, and therefore had radial seams. Model B was made of strips so arranged that the resulting seams were parallel and oriented at 45° to the polarization during tests. (See fig. 31.)

In testing, two halves were tested back-to-back and designated as, for example, Model A/C, which indicates that the Model A half is being tested while backed with the Model C half (fig. 32).

Reflectivity Tests

General. - At present, the theory (refs 9, 10, and 11) explaining the rf penetration effect has not been well-substantiated by experimental results, nor its existence proved in the lenticular configuration. Therefore, the following reflectivity measurements were performed.

Test program. - Monostatic and bistatic measurements of radar reflectivity of the five-foot diameter models were performed at two X-band frequencies. The bistatic measurements were limited to a single angle of 20°. Except for the cases where Model A is backed by Model B and vice versa, measurements were made at five tilt or elevation angles. No tests were made with the tetrapod booms. Table X outlines the test program, showing numbers for data patterns contained in GER 12331.

Test range. - A 470-foot ground range satisfying the $\lambda/16$ phase criterion was used. Rf field probes over the aperture of the test model were conducted to maintain the amplitude variations to ±0.5 db. The range was operated clockwise, with the klystron phase locked to a reference crystal-controlled oscillator to maintain frequency stability. Horizontally polarized 42-inch and 51-inch diameter parabolas were used as transmitting and receiving antennas, respectively.

The target support was a polystyrene foam (1.5 lb/ft^3) post, 5-1/2 feet high and 11.7 inches in diameter. A single axis gimbal system at the top allowed tilt or elevation movement of the A/C and B/C models. In all cases, the two halves of each model were pinned together with dielectric pins. In the case of the A/B and B/A tests, the pin extended through the back

of the model into a plywood crescent. This crescent then bolted to the top of the foam post in place of the gimbal system (see fig. 33).

Range and level calibration reference targets were four cylinders ranging in length from 12 inches to 30 inches. These references were mounted on the support post with a special cap. The support post was mounted on an azimuth rotator on a platform stand. A wall of CV-6 (Emerson-Cuming) absorber was inclined in front of the mount to reduce its return (see fig. 34).

Test procedure. - The procedure followed in recording the model radar reflectivity is indicated below.

(1) Extraneous background was reduced to a minimum and recorded.

(2) Return of the 30-inch and 12-inch long reference cylinders was recorded.

(3) Background level was reduced to ensure system stability.

(4) Model return (all five tilt angles on Models A/C and B/C) was recorded.

(5) Background return was recorded.

(6) Return from 30-inch reference cylinder was recorded to assure overall system stability during model measurements.

This procedure was followed for all reflectivity patterns recorded; hence, a set of patterns is needed to comprise any given measurement. The background noise level was at least 20 db below the peak model return level, except in a few isolated cases over limited angular regions.

All patterns were recorded with the model rotating in a clockwise (looking down on mount from above) direction. The pattern recording begins on the right-hand side of the paper under the title block. No attempt was made to reference the pattern zero in any fixed direction.

Results and data analysis. -

Monostatic: The mean levels of the backscattered radiation are approximately equal to the reference level (30-inch cylinder) for 0°, 10°, 20°, and 30° tilts. For the 40° tilt the level is down 6 to 8 db. Data patterns are given in GER 12331. A strong center interaction appears at the 0° tilt and to a lesser extent in the 10°, 20°, and 30° tilts. It is characterized by sharp deep nulls at $\pm9^o$ for the solid reflector backed models (A/C and B/C), but in the tests of the A/B and B/A models the nulls occur at $\pm12^o$ (see pattern on page 18).

The sector between the nulls changes mean level, depending on model and frequency. In all cases, the return is characterized by scintillations about the mean level of approximately 6 db magnitude. It must be noted that the returns of all Phase III models have the same edge diffraction scintillation characteristics at the center of response as the solid reflecting model of Phase I (see fig. 35).

20° Bistatic: The 20° bistatic return for all Phase III models is quite similar to the solid Phase I model. Mean return levels for 0°, 10°, 20°, and 30° tiles is approximately 2 db less than the reference (30-inch cylinder). Amplitude variations are small, ±2 db. Model B/C shows the edge diffraction interaction at both frequencies and has a center dip at 20° tilt.

Models A/C and B/C   Models A/B and B/A

-9°   0°   +9°   -12°   0°   +12°
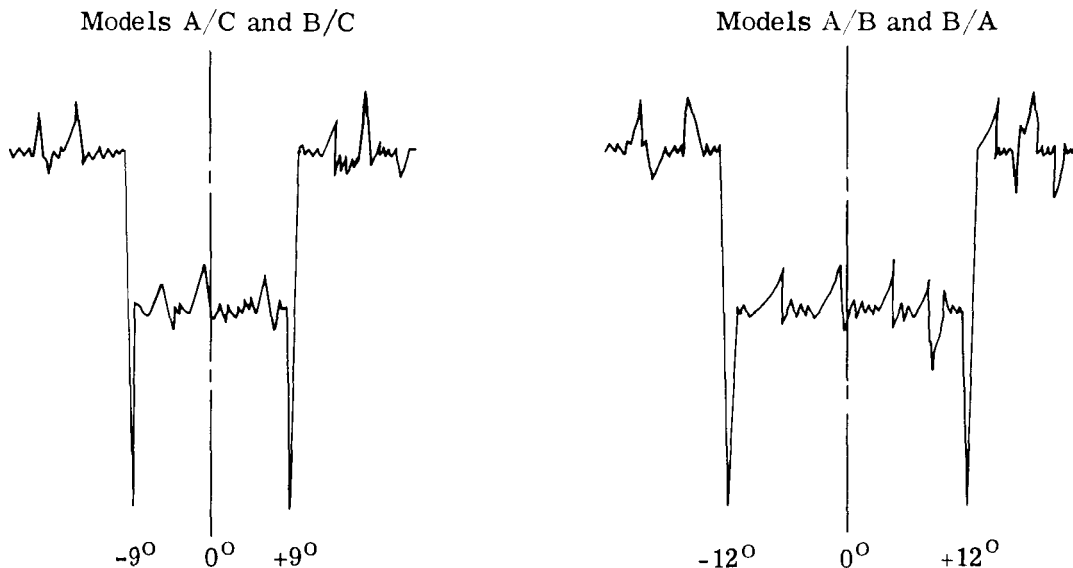
Model A/C shows these interactions at 9263 Mc only. The mean return levels for 40° tilt is 3 to 9 db below reference level. Data patterns are included in GER 12331.

Comparison of Phase I and Phase III: A comparison of the Phase I and Phase III data is given in the plots shown in figures 36 through 41. In each plot the relative mean radar cross sections are presented. Each has been normalized to the peak cross section of the 30-inch long reference cylinder.

Conclusions

In general, the return from Model A/C with the polar on radial gores was very slightly lower than the return from Model B/C with the equatorial parallel gores, although the difference was almost within the area of possible experimental error. The A/B and B/A test showed that either grid material at the rear surface acted essentially the same as a continuous conductive sheet.

CONCLUSIONS AND RECOMMENDATIONS

The tests confirmed that diffraction interference is present and that interference reflection characteristics in general conform with theory. The maximum interference angle, measured with respect to the central axis of the lenticular cap, was 12 degrees. This 12-degree diffraction interference angle would be intolerable for an operational satellite. However, it is expected that the diffraction interference angle will decrease in direct proportion with the satellite diameter and frequency. Scaling in the above manner results in an expected diffraction return interference angle of 0.22 and 1.0 degree for a 267-foot satellite operating at 9000 and 2000 Mc respectively.

18

In future testing, satellite reflectivity tests should be conducted using an inflated satellite that has a small diffraction interference angle or signal amplitude. This would reduce diffraction-caused scintillation and simplify the measurement of the lenticular cap bistatic reflection characteristic. For this test the inflated wire grid satellite should have as large a diameter-to-wavelength ratio as practicable.

Before further work is undertaken on actual grid material models, the seam effect and other effects such as wrinkling of the model need to be more thoroughly understood. Data resulting from the Phase II studies indicated that the type of seam used on the models should have no effect. However, some interaction takes place whenever a surface is constructed of grid material seamed together. Possibly some reflectivity tests should be made of some type of panel or sample, large in terms of wave lengths, where material wrinkling could be controlled. These might start out with no seams and gradually build up in seam number and gore patterns.

TABLE I. - FULL SCALE AND SCALE MODEL PARAMETERS*

Parameter	Full Scale	Scale Model
Radius of curvature (lens)	200 ft	4 ft
Truncation diameter	267 ft	5 ft
Boom length	210 ft	3.93 ft
Boom radius	2 in.	0.44 in.
Lens radar cross section	12.6×10^4 sq ft	50.3 sq ft
Boom cross section (broadside)	9.67×10^4 sq ft	33.2 sq ft
Spherical included angle	84°	77.5°
Angle from vertical of peak boom return	= 50.5°	= 50.5°
Canister diameter	56 in.	--
Canister cross section	17.1 sq ft	--
Frequency	2000 Mc	9500 Mc
Wave Length	5.9 in.	1.2 in.

*Model scale factor = 5/267 = 0.0187.

TABLE II. - LIST OF MATERIALS

Material	Description	Supplier	Used in Phase
E293-481-I 550	Epoxy preimpregnated fiberglass cloth	Cordo Division of Ferro Corporation Norwalk, Connecticut	I
Silver Powder M-103	Silflake 135	Handy & Harman New York, New York	I, II, III
Vitel PE-207	Polyester resin	Goodyear Tire & Rubber Company Akron, Ohio	II, III
Metal Foil	3-mil tempered aluminum	--	II
Epon 828	Epoxy resin	Shell Chemical Company New York, New York	I
Versamid 125	Amine-terminated polyamide	General Mills Corporation Chemical Division Minneapolis, Minnesota	I
Schjeldahl GT-300 Tape	Mylar film + polyester resin	G.T. Schjeldahl Co Northfield, Minnesota	II, III
Close Mesh Grid	80 x 80 x 0.0055" woven wire cloth, phosphor bronze - plain	Unique Wire Weaving Co Hillside, New Jersey	II, III
Temp-R-Tape C	Thermal-curing pressure-sensitive FEP Teflon tape (0.003" total thickness) 1/2" wide	The Connecticut Hard Rubber Company New Haven, Connecticut	II, III
Plastilock 604 Adhesive	Thermosetting adhesive	B.F. Goodrich Akron, Ohio	II
Lenticular Grid Material	1.6-mil phosphor bronze wire 24 x 24 cloth mesh 0.7-mil photolyzable film	--	II, III
Medium Mesh Grid	3-mil aluminum wire with 0.025" spacing in both directions (40/inch) 2 ply, 1/2-mil Mylar Tape C; clear PE-207 Vitel resin	Goodyear Aerospace Corp. Akron, Ohio	II

TABLE III. - FORMULATIONS USED

Item	Element	Parts by Weight
Adhesive - Phase I Model (Joining of two halves)	Epon 828 Versamid 125 Cabosil Glycerol	60.0 40.0 5.0 1.0
Silver-Loaded Polyester Resin (Conductive material)	M-103 Vitel PE-207 PAPI Toluene	60.0 40.0 4.4 200.0
Rigid Polyurethane Foam	Plaskon PFR No. 6 DABCO LV-33 Silicone 5310 Trichloromonofluoromethane Nacconate 1080 HM	100.0 0.33 1.0 32.0 110.0

TABLE IV. - SUMMARY OF RF TEST PROGRAM FOR FIVE-FOOT DIAMETER MODEL

Frequency	Tilt Angle (deg)	Monostatic Angle		Bistatic Angle							
				20°			40°		60°		
		WB	W_0B	WB	W_0B	WB_s	WB	W_0B	WB	W_0B	WB & Sail
8669 Mc	(Ref. Patt)*	I-1	I-7	I-61	I-67		I-127	I-133	I-187	I-193	
	0	-2	-8	-62	-68		-128	-134	-188	-194	
	10	-3	-9	-63	-69		-129	-135	-189	-195	
	20	-4	-10	-64	-70		-130	-136	-190	-196	
	30	-5	-11	-65	-71		-131	-137	-191	-197	
	40	-6	-12	-66	-72		-132	-138	-192	-198	
8843 Mc	(Ref. Patt)	I-13	I-19 -19A	I-73	I-79		I-139	I-145	I-199	I-205	
	0	-14	-20	-74	-80		-140	-146	-200	-206	
	10	-15	-21	-75	-81		-141	-147	-201	-207	
	20	-16	-22	-76	-82		-142	-148	-202	-208	
	30	-17	-23	-77	-83		-143	-149	-203	-209	
	40	-18	-24	-78	-84		-144	-150	-204	-210	
8993 Mc	(Ref. Patt)	I-25	I-31	I-85	I-91		I-151	I-157	I-211	I-217	
	0	-26	-32	-86	-92		-152	-158	-212	-218	
	10	-27	-33	-87	-93		-153	-159	-213	-219	
	20	-28	-34	-88	-94		-154	-160	-214	-220	
	30	-29	-35	-89	-95		-155	-161	-215	-221	
	40	-30	-36	-90	-96		-156	-162	-216	-222	
9127 Mc	(Ref. Patt)	I-37	I-43	I-97	I-103		I-163	I-169	I-223	I-229	
	0	-38	-44	-98	-104		-164	-170	-224	-230	
	10	-39	-45	-99	-105		-165	-171	-225	-231	
	20	-40	-46	-100	-106		-166	-172	-226	-232	
	30	-41	-47	-101	-107		-167	-173	-227	-233	
	40	-42	-48	-102	-108		-168	-174	-228	-234	
9263 Mc	(Ref. Patt)	I-49	I-55	I-109	I-115	I-121	I-175	I-181	I-235	I-241	I-247
	0	-50	-56	-110	-116	-122	-176	-182	-236	-242	-248
	10	-51	-57	-111	-117	-123	-177	-183	-237	-243	-249
	20	-52	-58	-112	-118	-124	-178	-184	-238	-244	-250
	30	-53	-59	-113	-119	-125	-179	-185	-239	-245	-251
	40	-54	-60	-114	-120	-126	-180	-186	-240	-246	-252

WB   - With tetrapod booms
W_0B - Without tetrapod booms
WB_s - With small booms
WB & S - With booms and solar sail

*Reference patterns are included with these identifications in GER 12331 (see Foreword).

TABLE V. - REFERENCE CYLINDERS (MONOSTATIC)

Length (ft)	Cross Section (Sq Ft)					Relative Cross Section (db)
	8869 Mc	8843 Mc	8993 Mc	9127 Mc	9263 Mc	
1.0	8.04	8.20	8.35	8.48	8.60	-7.96
1.5	18.0	18.4	18.7	19.0	19.3	-4.45
2.0	32.1	32.8	33.4	33.9	34.4	-1.94
2.5	50.2	51.2	52.1	52.9	53.7	0.00

TABLE VI. - MATERIALS DEFINITION - SEAM TEST MODELS

Material Type	Physical Characteristics	Weight (lb/sq ft)
Metal Foil	3-mil aluminum foil (tempered)	0.036
Close-Mesh Grid*	80 x 80 wires per inch 5.5-mil phosphorous bronze wire	0.16
Lenticular Grid	24 x 24 wires per inch 1.6-mil phosphorous-bronze wire in 0.7-mil clear photolyzable film	0.008
Medium-Mesh Grid (Extra test material)	40 x 40 wires per inch 3-mil aluminum wire Laminated between 1/2-mil Mylar each side	0.034

*This material was commercially available, and although too heavy for satellite use, was a suitable close-mesh grid for rf data comparison purposes.

TABLE VII. - MATERIAL TEST DATA - SEAM TEST MODELS

Seam Sample No.	Material Type	Seam Adhesive*	Seam Type**	Seam Adhesive Type	Wire Orientation***
I-1	Metal Foil	NC	A		
I-2	Metal Foil	NC	B	1/2-mil Plastilock on 1/2-mil Mylar	
I-3	Metal Foil	NC	C		
I-4	Metal Foil	NC	D		
II-1	Metal Foil	C	A		
II-2	Metal Foil	C	B		
II-3	Metal Foil	C	C	1/2-mil Plastilock on 1/2-mil Mylar, plus silver-loaded Vitel resin	
II-4	Metal Foil	C	D		
II-5	Metal Foil	C	E		
III-1	Close Mesh Grid	NC	A		W
III-2	Close Mesh Grid	NC	B		W
III-3	Close Mesh Grid	NC	C	1/2-mil Schjeldahl GT-300 tape	W
III-4	Close Mesh Grid	NC	D		W
III-5	Close Mesh Grid	NC	E		W
IV-1	Close Mesh Grid	C	A		W
IV-2	Close Mesh Grid	C	B	1/2-mil Schjeldahl GT-300 tape plus silver-loaded Vitel resin	W
IV-3	Close Mesh Grid	C	C		W
IV-4	Close Mesh Grid	C	D		W
V-1	Close Mesh Grid	NC	A		X
V-2	Close Mesh Grid	NC	B	1/2-mil Schjeldahl GT-300 tape	X
V-3	Close Mesh Grid	NC	C		X
V-4	Close Mesh Grid	NC	D		X
VI-1	Close Mesh Grid	C	A		X
VI-2	Close Mesh Grid	C	B	1/2-mil Schjeldahl GT-300 tape plus silver-loaded Vitel resin	X
VI-3	Close Mesh Grid	C	C		X
VI-4	Close Mesh Grid	C	D		X
VII-1	Lenticular Grid	NC	A		Y
VII-2	Lenticular Grid	NC	B		Y
VII-3	Lenticular Grid	NC	C	Temp-R-Tape C	Y
VII-4	Lenticular Grid	NC	D		Y
VII-5	Lenticular Grid	NC	E		Y
VIII-1	Lenticular Grid	C	A		Y
VIII-2	Lenticular Grid	C	B	Temp-R-Tape C plus silver-loaded Vitel resin	Y
VIII-3	Lenticular Grid	C	C		Y
VIII-4	Lenticular Grid	C	D		Y
IX-1	Lenticular Grid	NC	A		Z
IX-2	Lenticular Grid	NC	B	Temp-R-Tape C	Z
IX-3	Lenticular Grid	NC	C		Z
IX-4	Lenticular Grid	NC	D		Z
X-1	Lenticular Grid	C	A		Z
X-2	Lenticular Grid	C	B	Temp-R-Tape C plus silver-loaded Vitel resin	Z
X-3	Lenticular Grid	C	C		Z
X-4	Lenticular Grid	C	D		Z
XI-1	Medium Mesh Grid	NC	B	Temp-R-Tape C	W
XI-2	Medium Mesh Grid	NC	C		W
XII-1	Medium Mesh Grid	C	B	Temp-R-Tape C plus silver-loaded Vitel resin	W
XII-2	Medium Mesh Grid	C	C		W

*NC - Nonconductive
C - Conductive
**Refer to table VIII.
***Refer to figure 21.

TABLE VIII. - SEAM TYPES
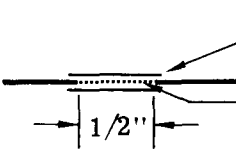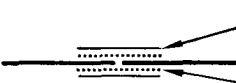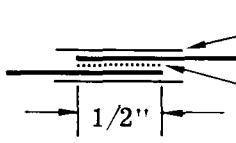
Designation	TYPE
A	1/2" Spacing between Segments 1-1/4" wide - 1/2-mil tape with 1/2-mil adhesive thickness 1/2" Conductive material used as indicated in table VII.
B	Butt 1/2" wide - 1/2-mil tape with 1/2-mil adhesive thickness Conductive material used as indicated in table VII.
C	1/2" Overlap 1-1/4" wide - 1/2-mil tape with 1/2-mil adhesive thickness 1/2" Conductive material used as indicated in table VII.
D	3/4" Overlap 1-1/4" wide - 1/2-mil tape with 1/2-mil adhesive thickness Conductive material used as indicated in table VII.
E	Continuous Reflecting Surface

TABLE IX. - PHASE II TESTS - MONOSTATIC CONDITION AT 8.843 Gc

Material	Nonconducting Adhesive					Conducting Adhesive				
	Ref.	1/2" Gap	Butt	1/2" Overlap	3/4" Overlap	Ref.	1/2" Gap	Butt	1/2" Overlap	3/4" Overlap
Metal Foil	II-1	II-2	II-3	II-4	II-5	II-6	II-7	II-8	II-9	II-10
80 x 80 Mesh Wires, Horizontal and Vertical	II-11	II-12	II-13	II-14	II-15	II-16	II-17	II-18	II-19	II-20
80 x 80 Mesh 45° Wires	II-21	II-22	II-23	II-24	II-25	II-26	II-27	II-28	II-29	II-30
Lenticular Grid Wires, Horizontal and Vertical	II-31	II-32	II-33	II-34	II-35	II-36	II-37	II-38	*	*
Lenticular Grid 45° Wires	II-41	II-42	II-43	II-44	II-45	II-46 II-46A	II-47	II-48	II-49	II-50
40 x 40 Mesh Wires, Horizontal and Vertical	II-51	*	II-52	II-53	*	II-56	*	II-57	II-58	*

*Samples not available for test

TABLE X. PHASE III TESTS

Model	Tilt Angle (deg)	Monostatic Frequency (Mc)		20° Bistatic Frequency (Mc)	
		8843	9263	8843	9263
A/C	(Ref. Patt)	III-1	III-7	III-13	III-19
	0	-2	-8	-14	-20
	10	-3	-9	-15	-21
	20	-4	-10	-16	-22
	30	-5	-11	-17	-23
	40	-6	-12	-18	-24
B/C	(Ref. Patt)	III-25	III-31	III-37, 37A	III-43
	0	-26	-32	-38	-44
	10	-27	-33	-39	-45
	20	-28	-34	-40	-46
	30	-29	-35	-41	-47
	40	-30	-36	-42	-48
A/B	(Ref. Patt)	III-50	III-52	III-54	III-56
	0	-51	-53	-55	-57
B/A	(Ref. Patt)	III-58	III-60	III-62	III-64
	0	-59, 59A	-61	-63	-65

Figure 1. - Rf analysis and testing of 20-inch diameter
lenticular satellite model (ref. 1).

Damper boom (extendible)

Yaw control boom (extendible)

Solar sail

Tetrapod booms

Rf reflecting lens
(267-ft diameter)

Tetrapod booms,
210-ft length

≈ 50 ft

Solar sail

Canister half and
miscellaneous hardware
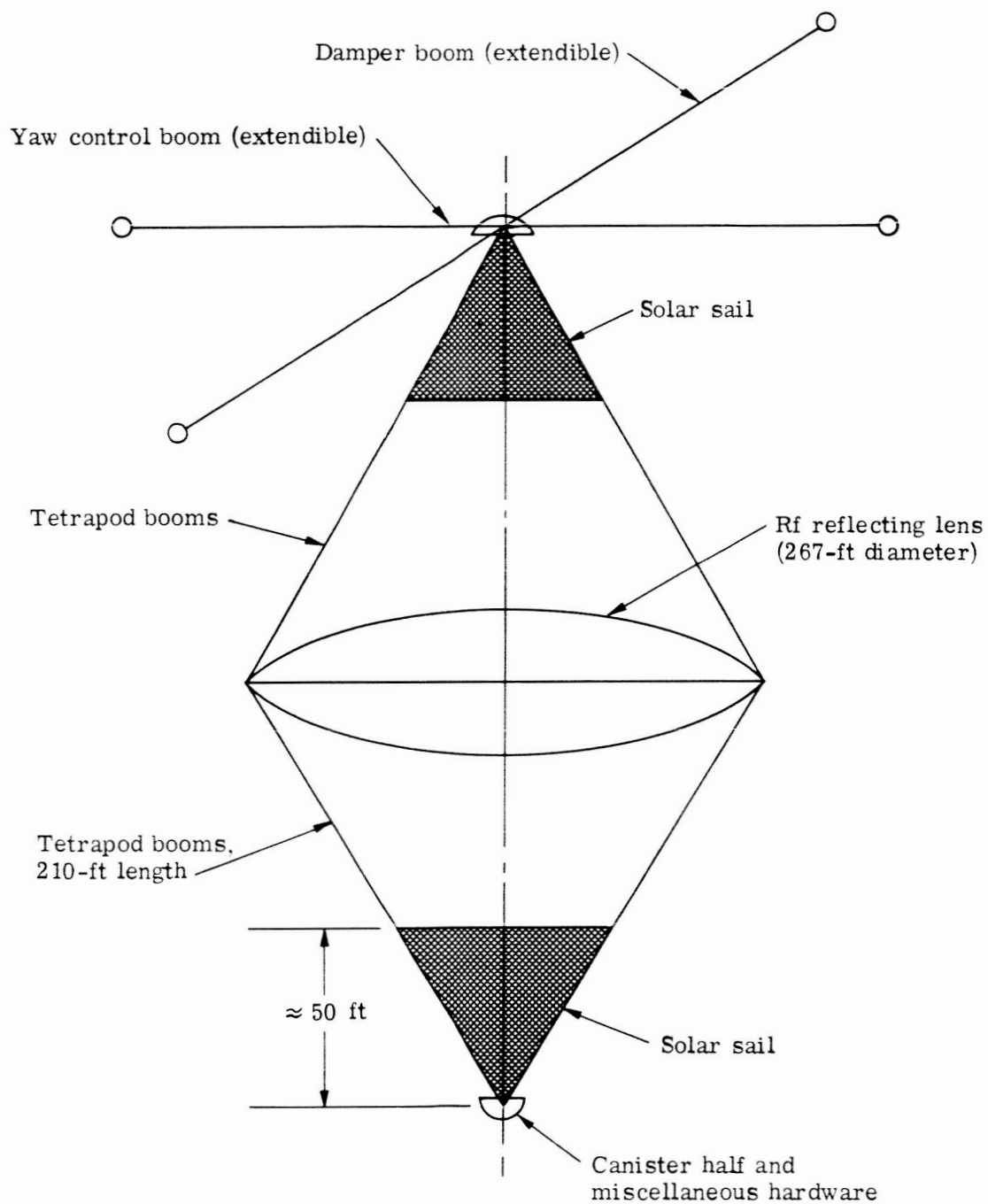
Figure 2. - Schematic of lenticular satellite with gravity-gradient stabilization.

Figure 3. – Five-foot diameter fiberglass rf test model with booms.
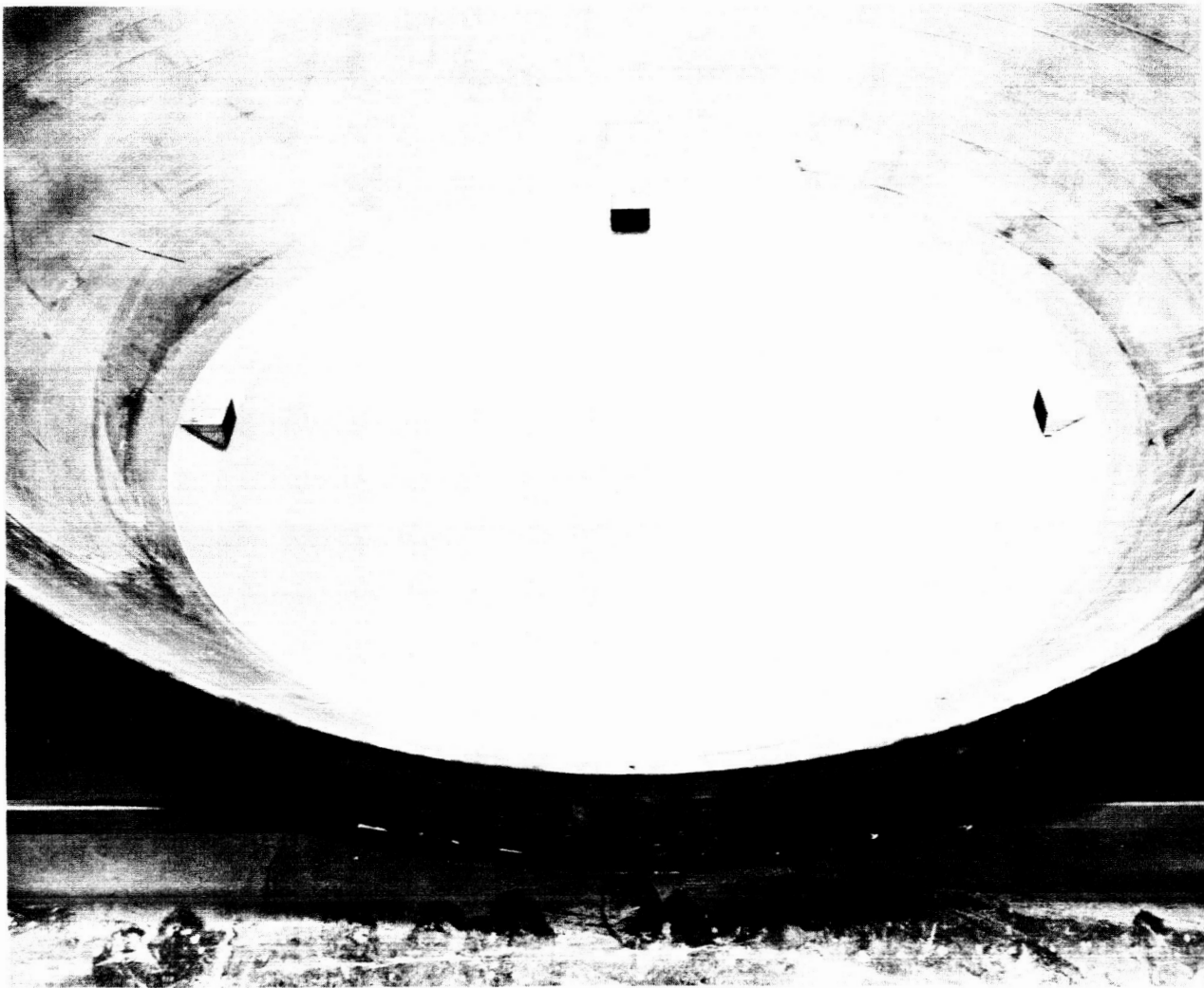
Figure 4. - One-half of five-foot diameter fiberglass model in mold.
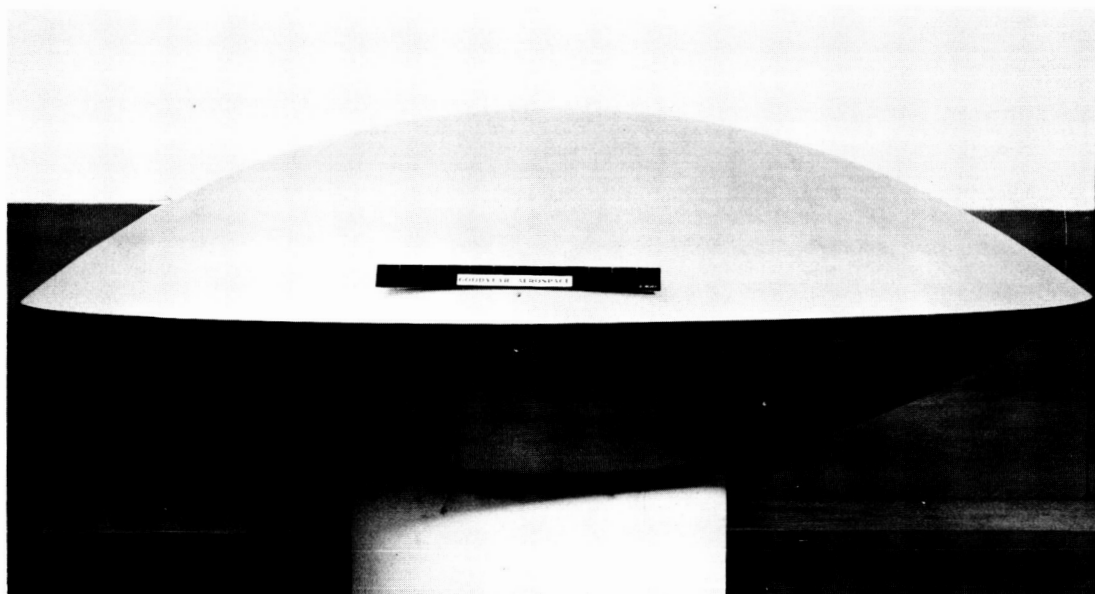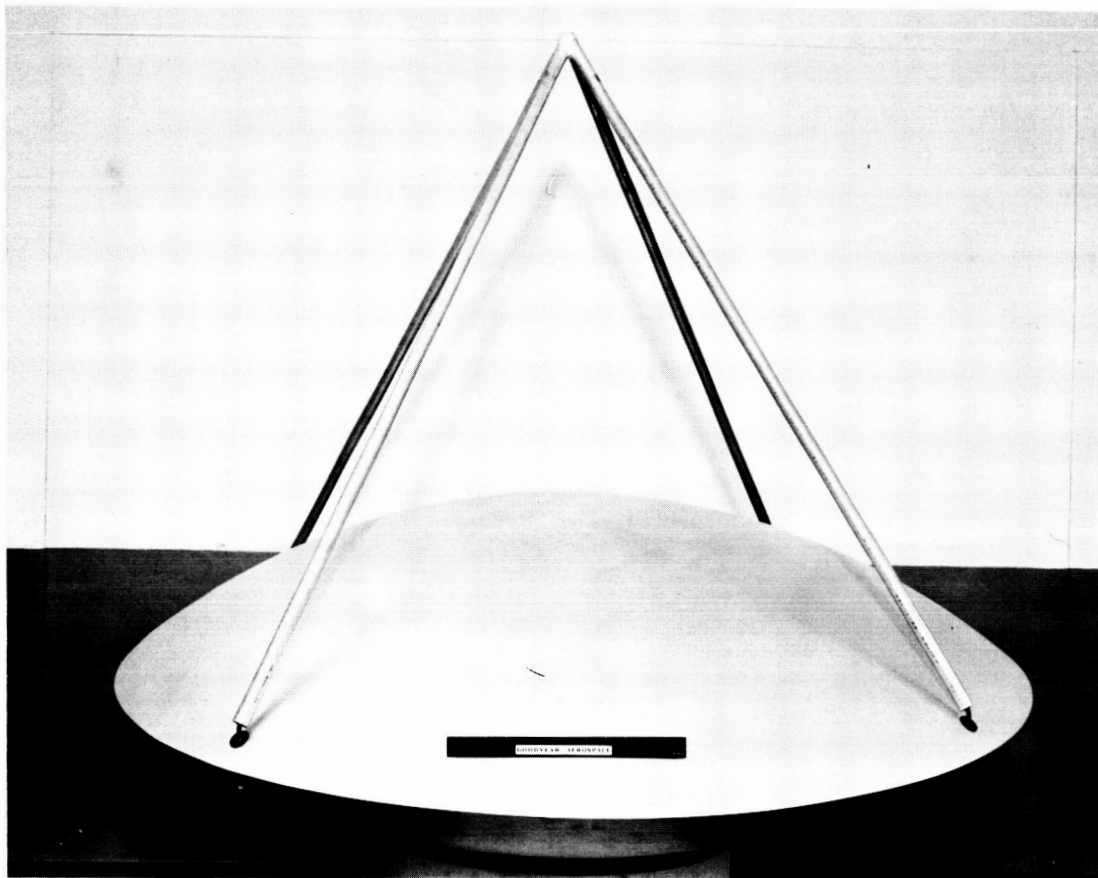
Figure 5. - Five-foot diameter fiberglass rf model with booms
and without booms.
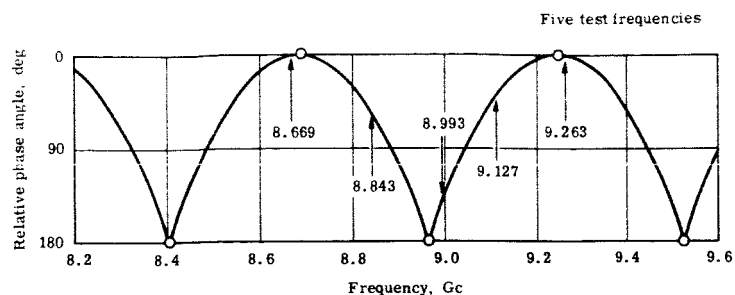
Figure 6. - Relative phase angle between specular and edge diffraction return.
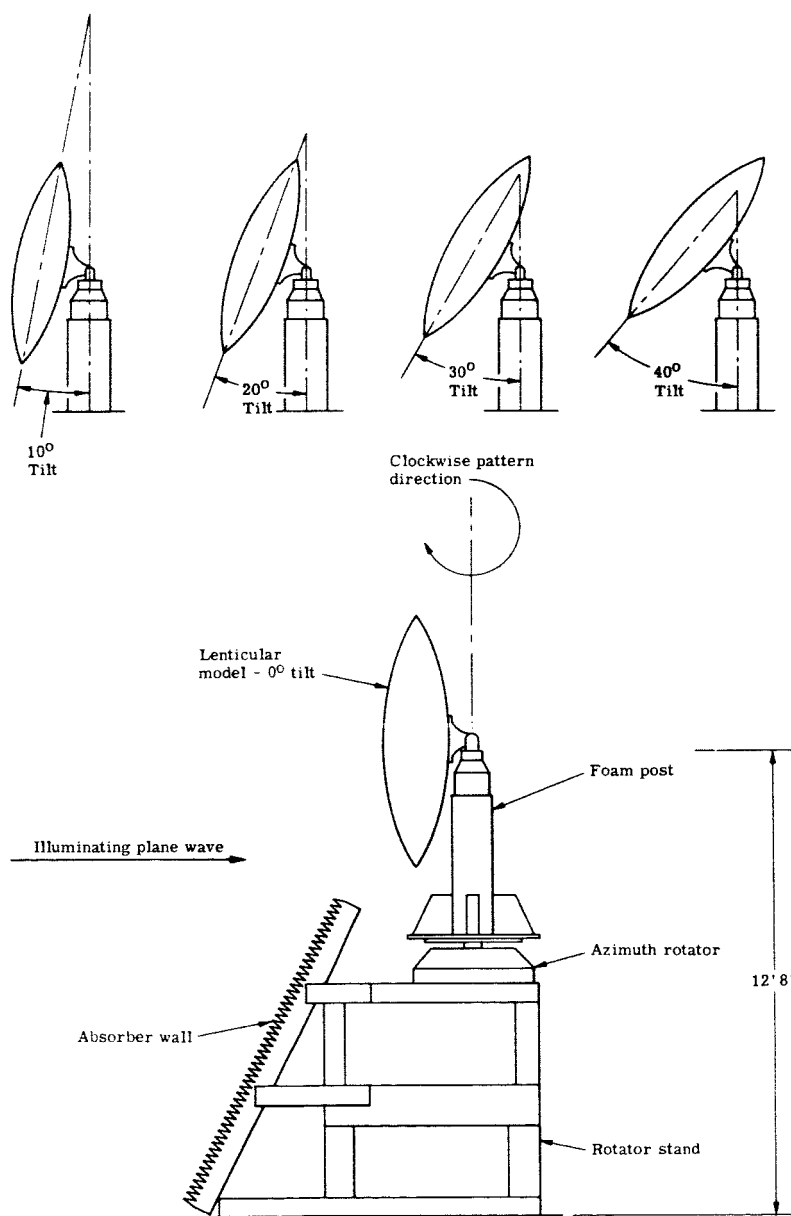
Figure 7. - Tilt positions and mounting scheme.

31
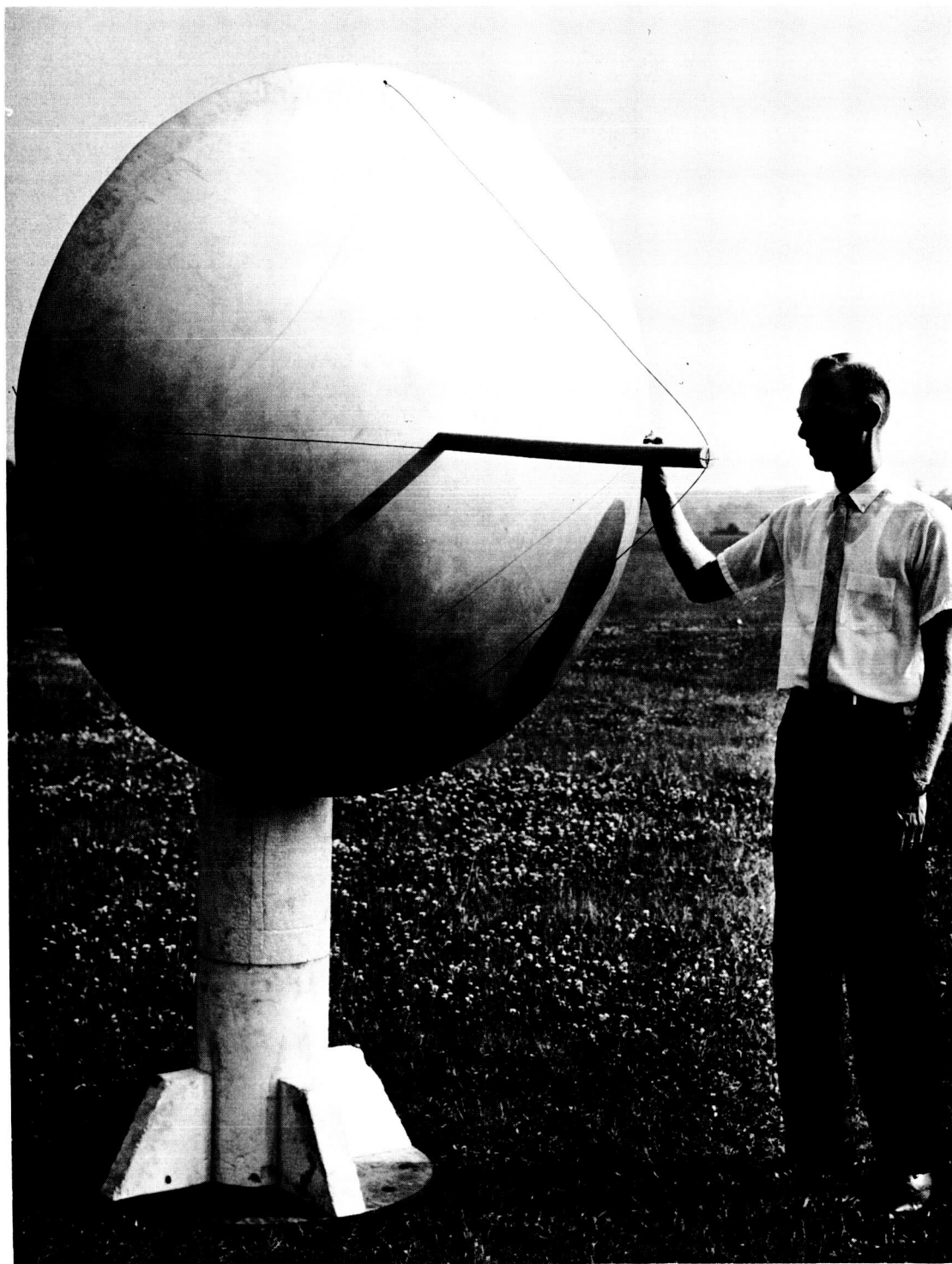
Figure 8. - Five-foot model with small booms.
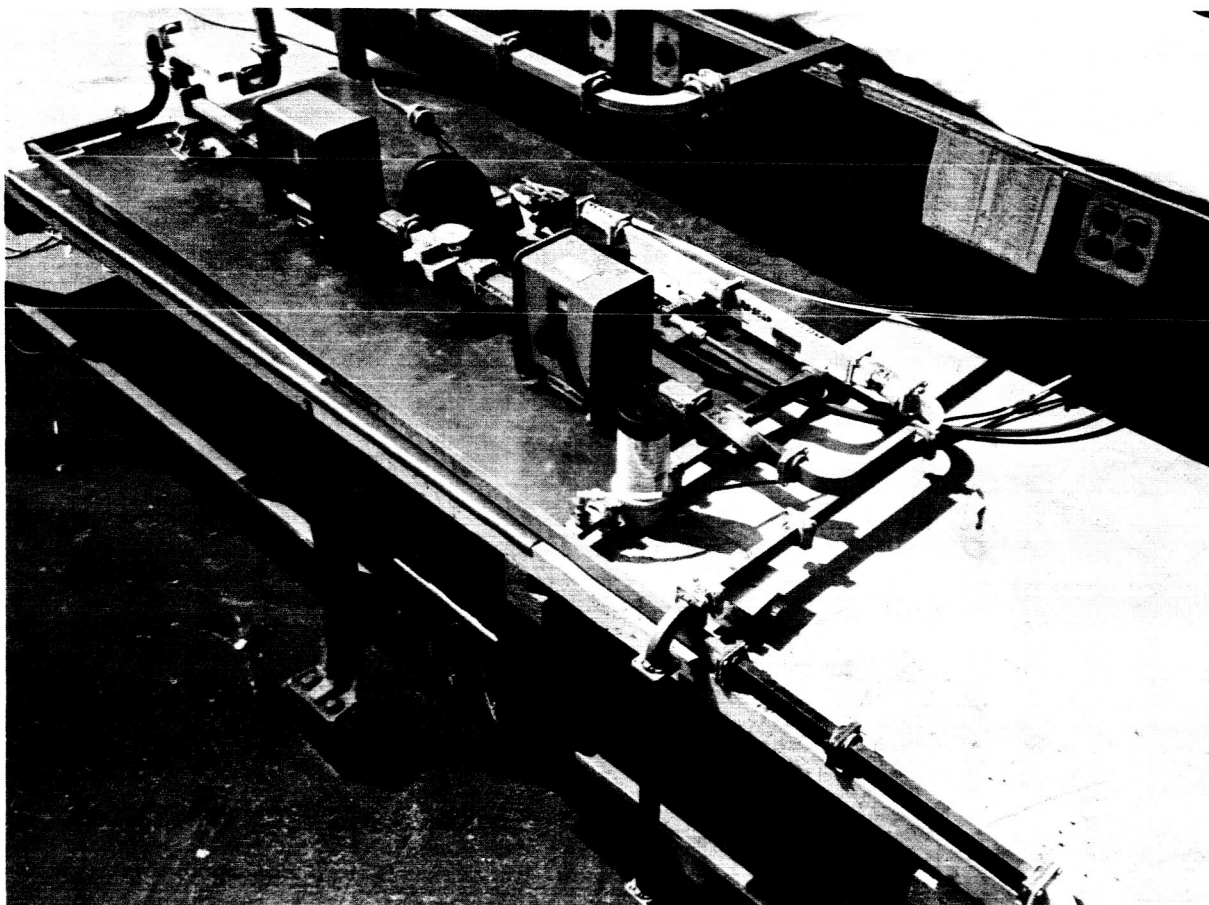
Figure 9. - Monostatic scattering measurement setup.
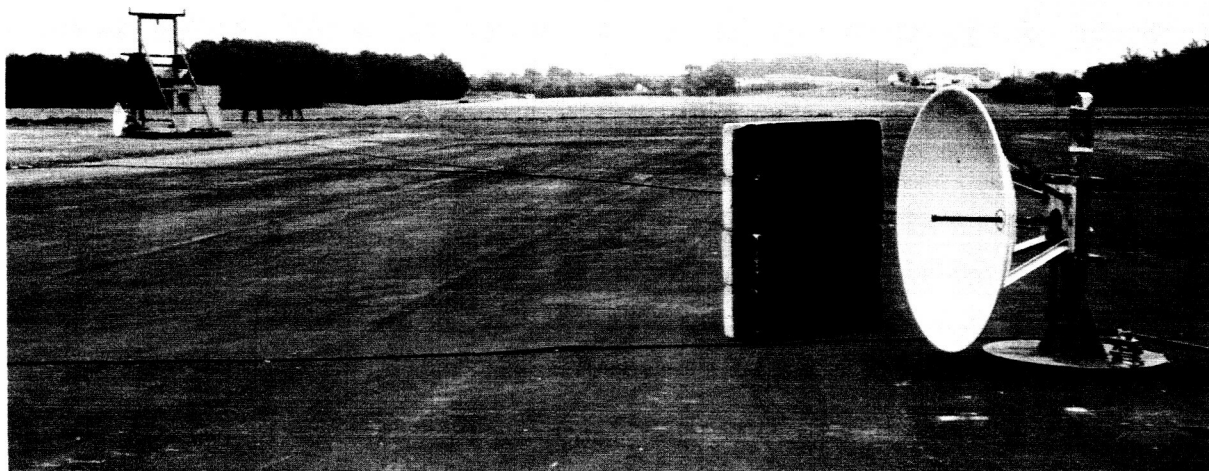
Figure 10. - Bistatic scattering measurement setup.
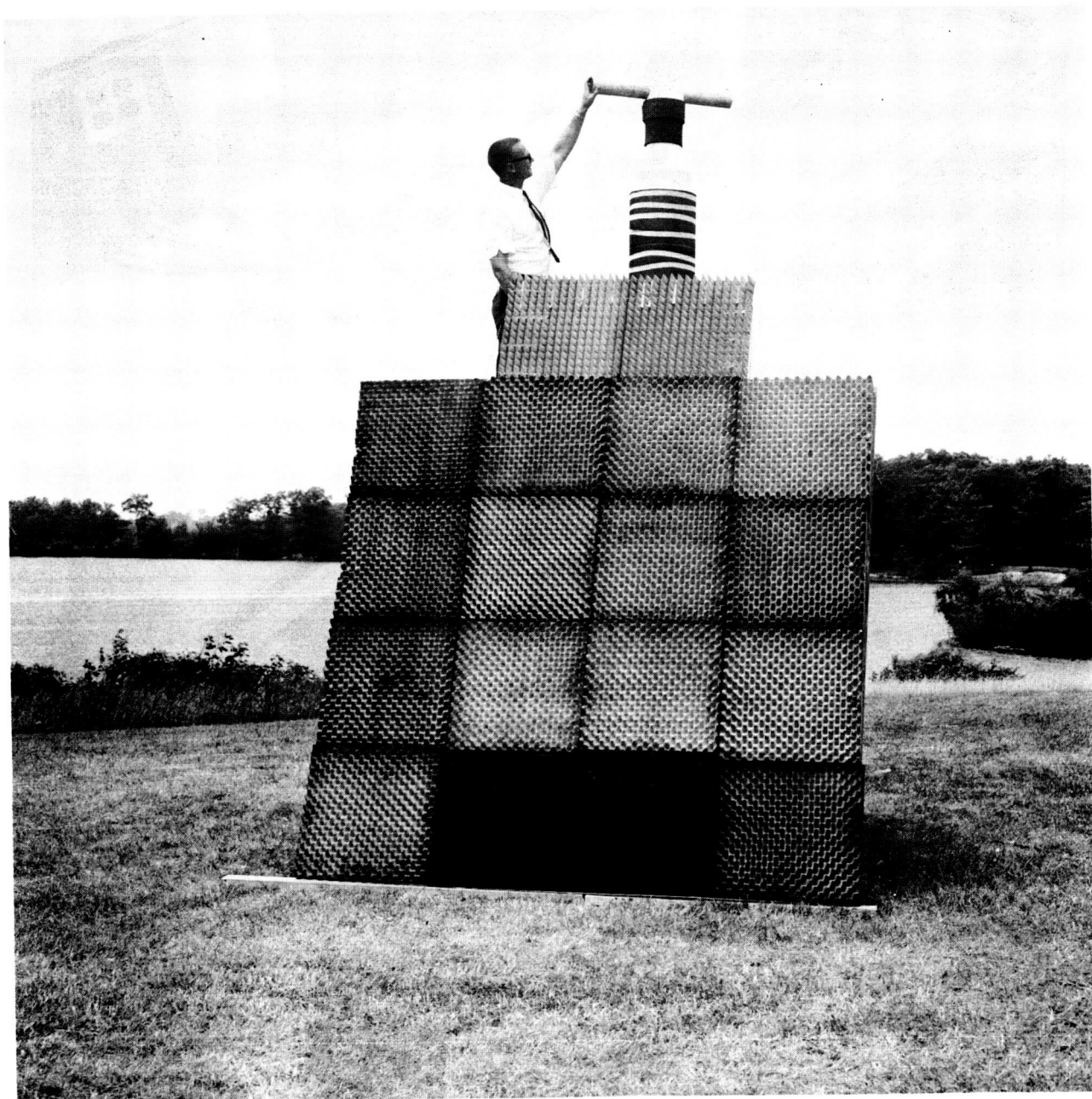
Figure 11. - Test stand.
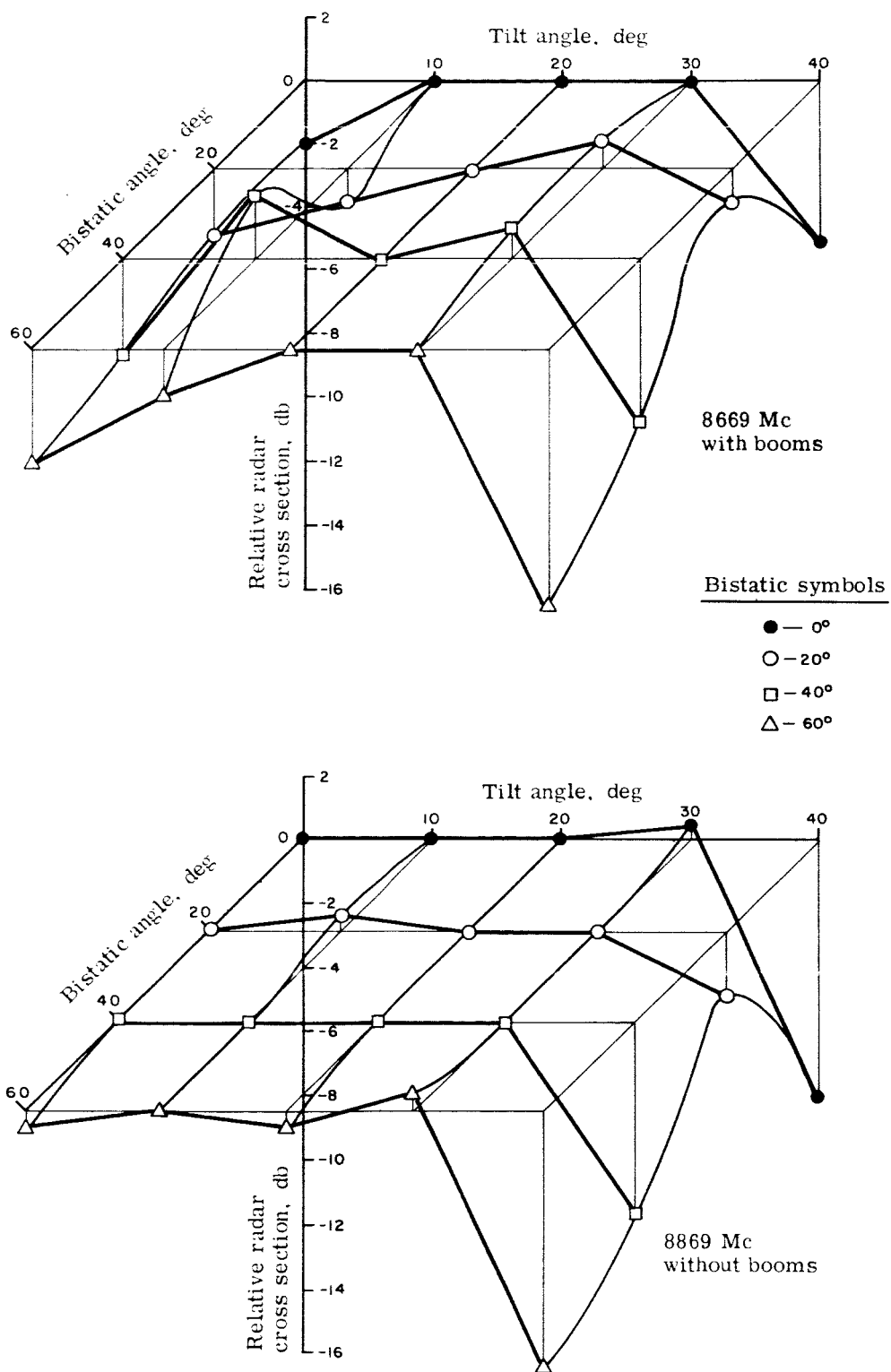
Figure 12. - Bistatic radar cross section of five-foot model at 8669 Mc.
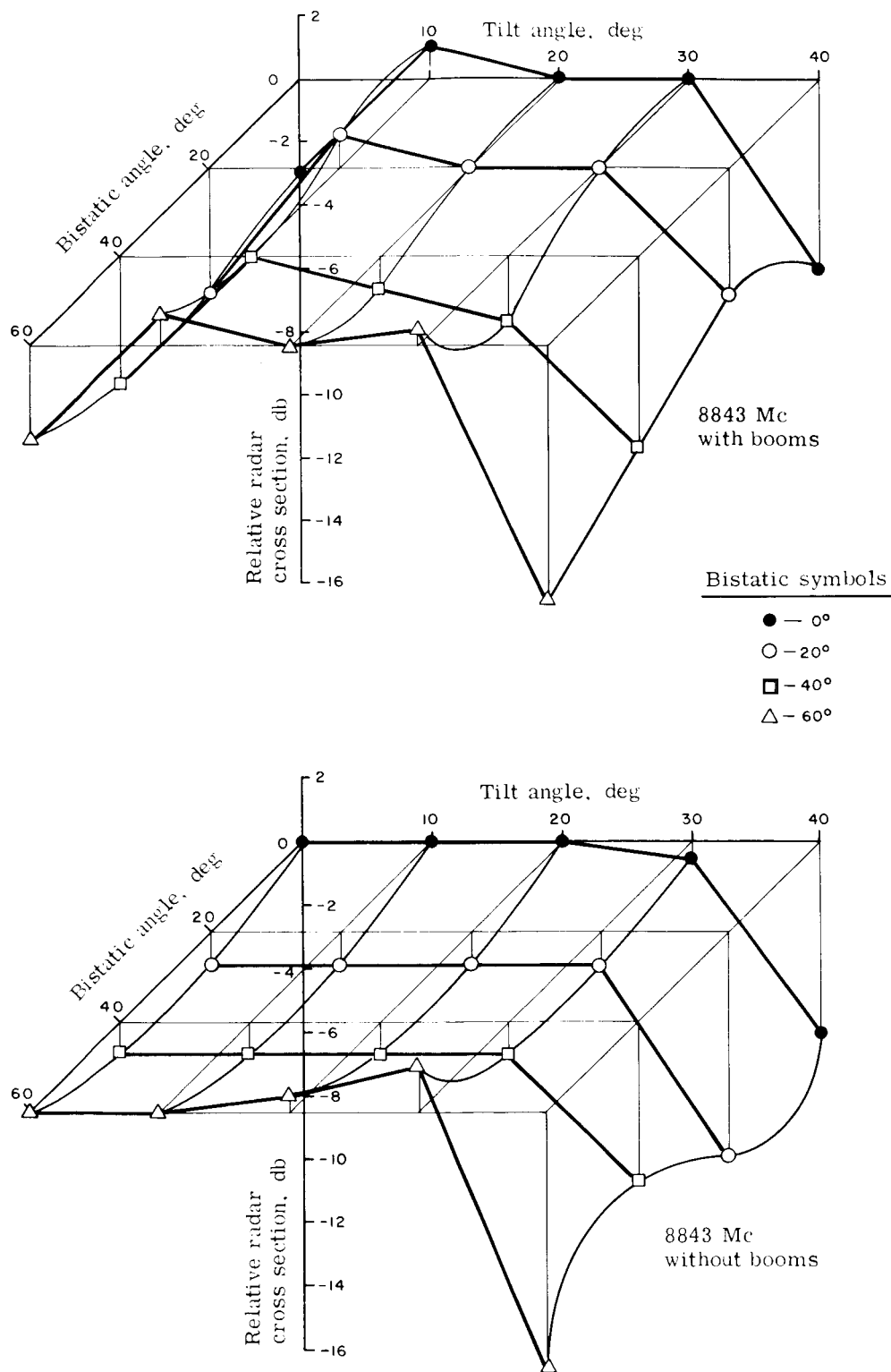
Figure 13. - Bistatic radar cross section of five-foot model at 8843 Mc.
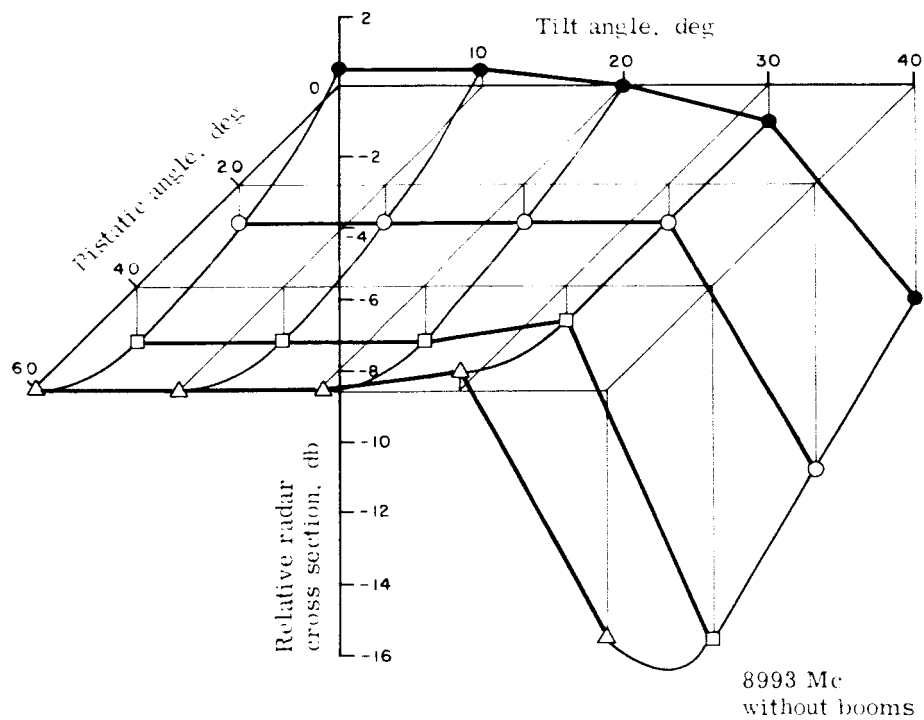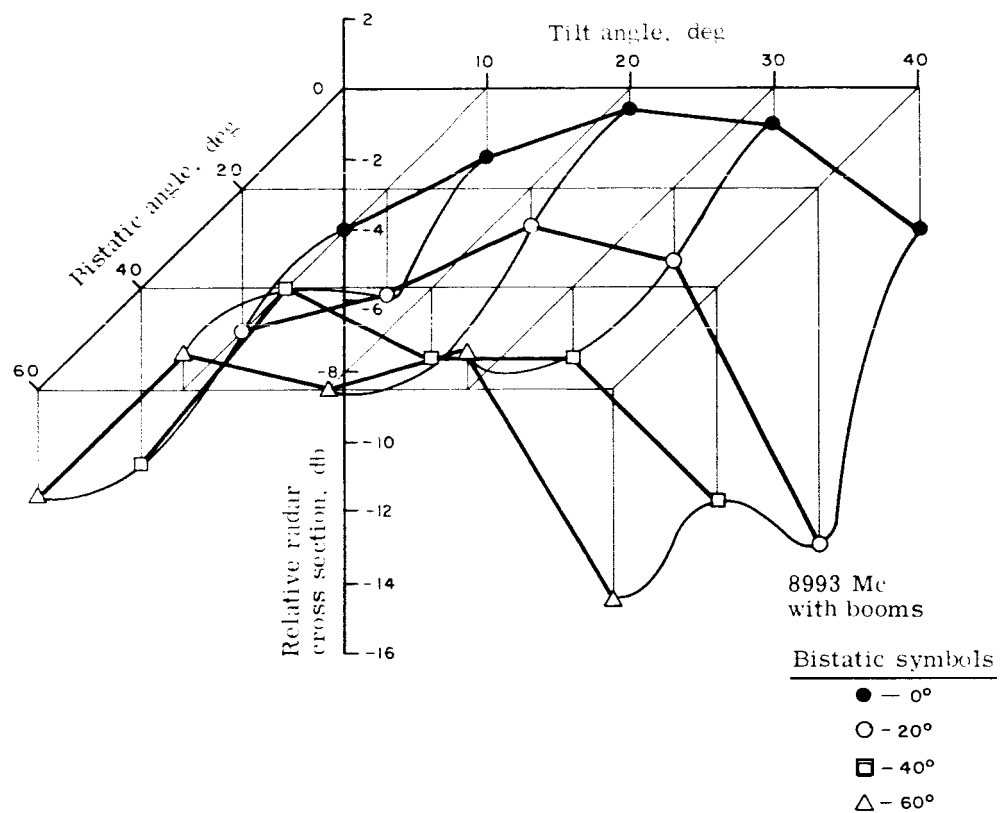
Figure 14. - Bistatic radar cross section of five-foot model at 8993 Mc.
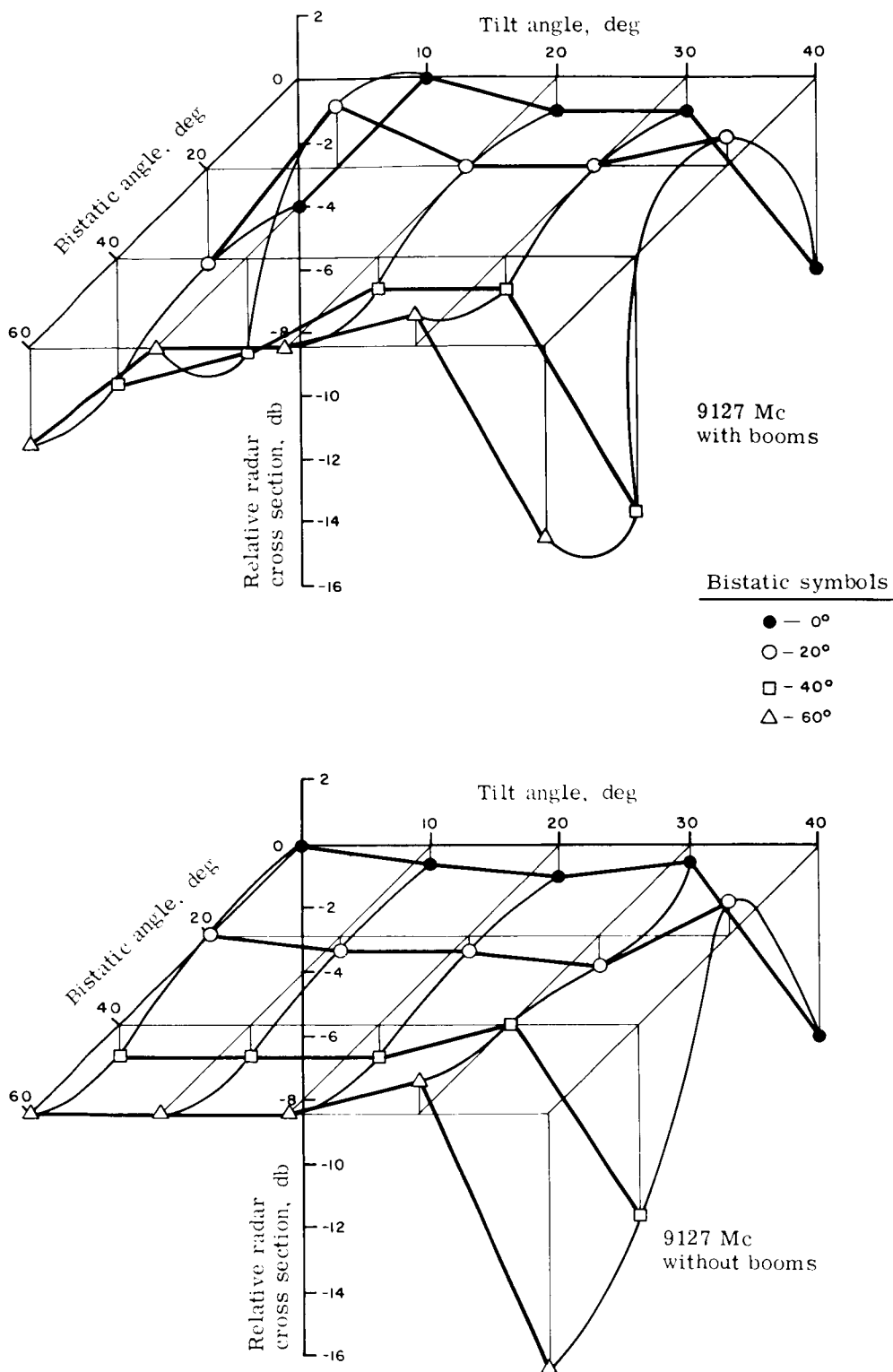
Figure 15. - Bistatic radar cross section of five-foot model at 9127 Mc.
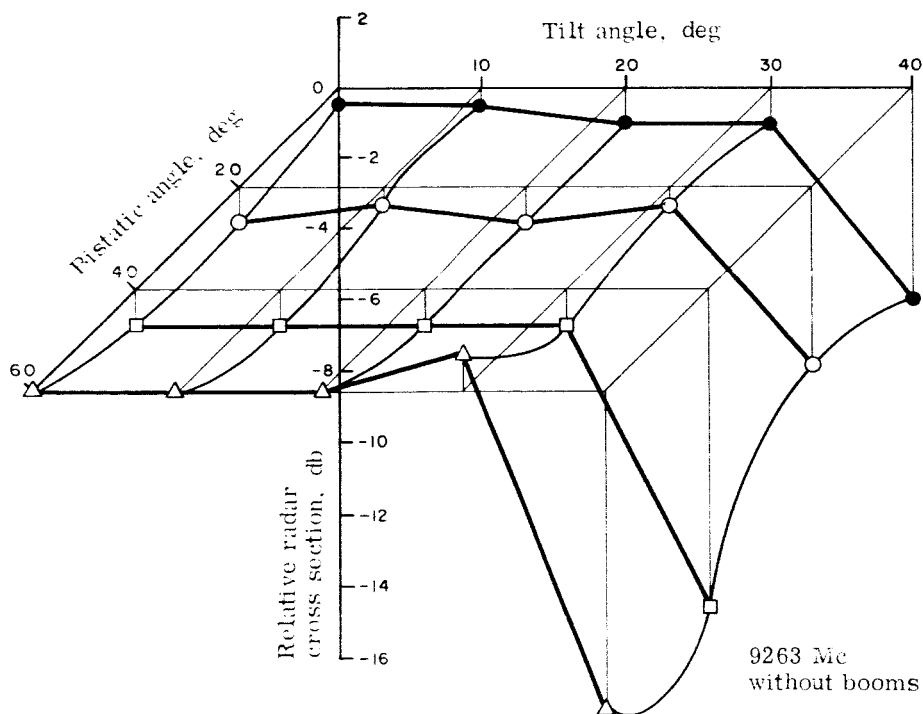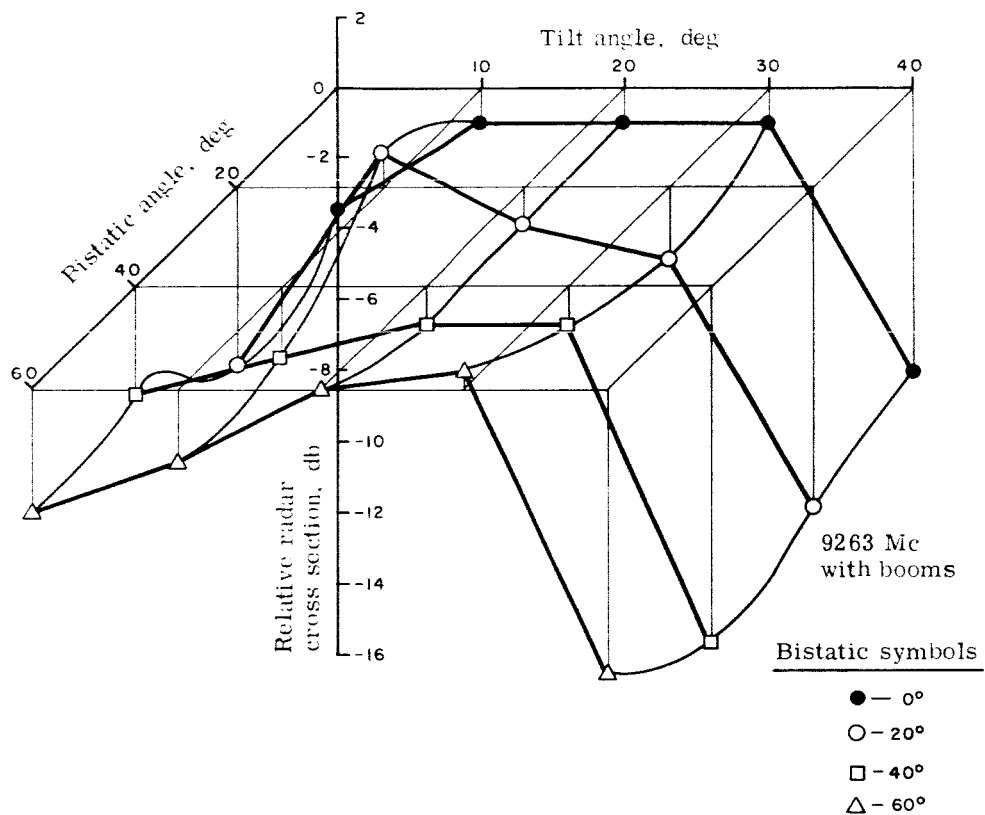
Figure 16. - Bistatic radar cross section of five-foot model at 9263 Mc.
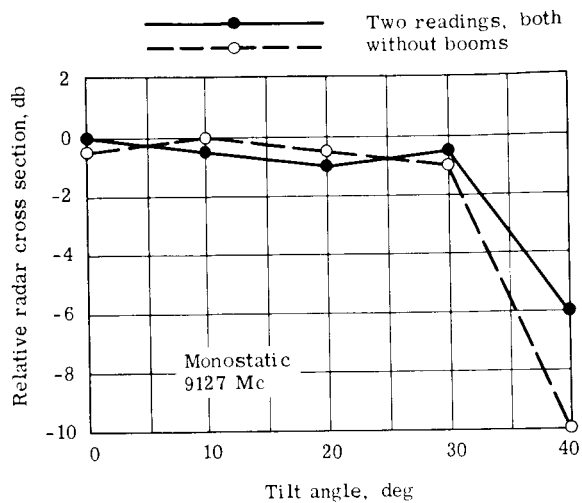
Figure 17. - Data repeat characteristics of radar cross section tests showing setup accuracy.
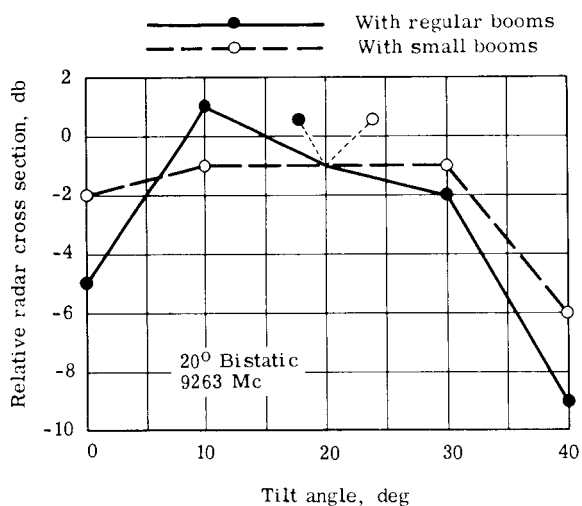
Figure 18. - Effect of tetrapod boom size on radar cross section of five-foot model.
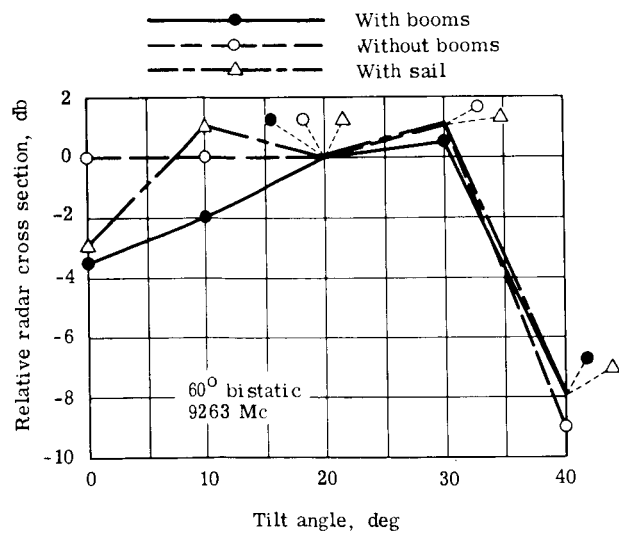
Figure 19. - Effect of representative solar sail on radar cross section of five-foot model with sail and booms.
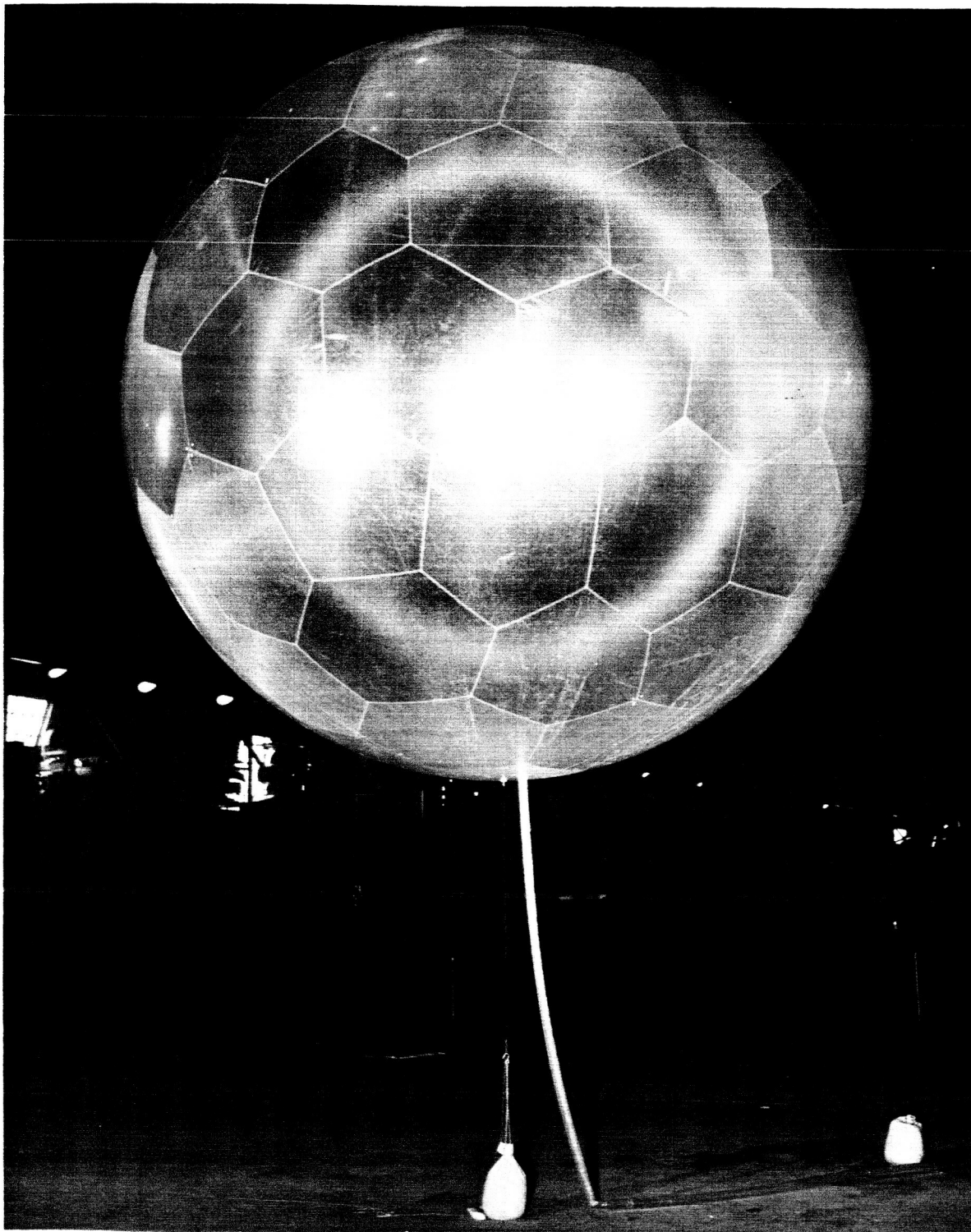
Figure 20. - Grid sphere.
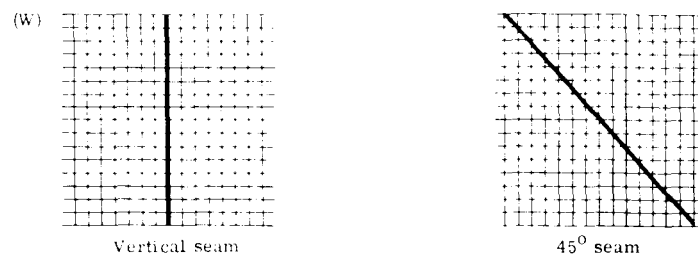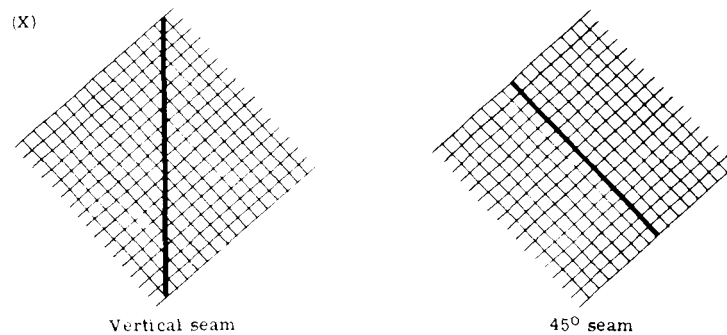
(W)

Vertical seam   45° seam

Solid line indicates single wire, uniformly spaced

(X)

Vertical seam   45° seam

Solid line indicates single wire, uniformly spaced

(Y)

Vertical seam   45° seam

Solid line indicates direction of grouped wiring
Dotted line indicates direction of single wire, uniformly spaced

(Z)

Vertical seam   45° seam
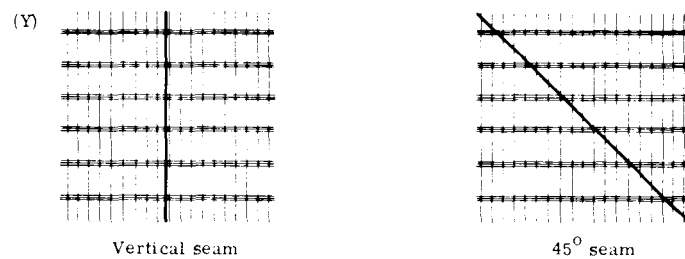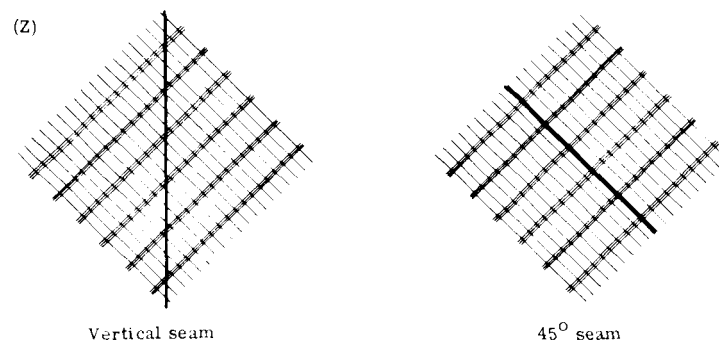
Solid line indicates direction of grouped wiring
Dotted line indicates direction of single wire, uniformly spaced

Figure 21. - Wire orientation of grid materials.
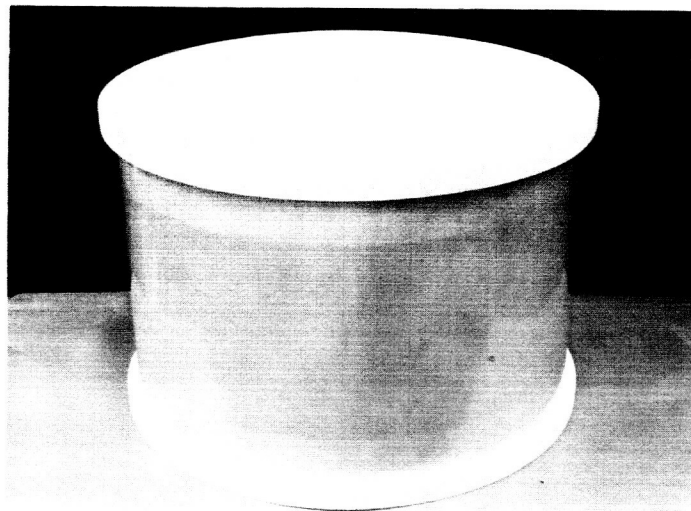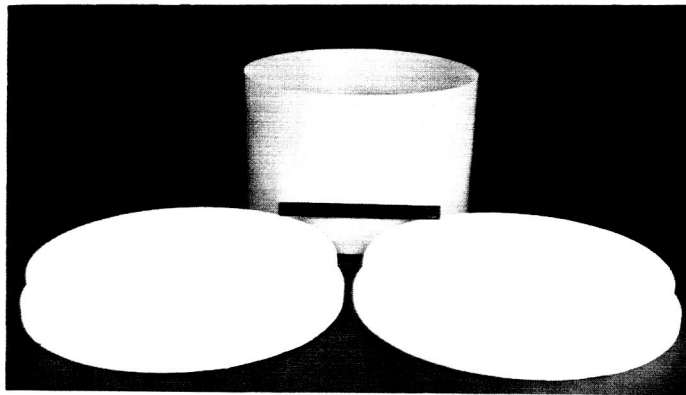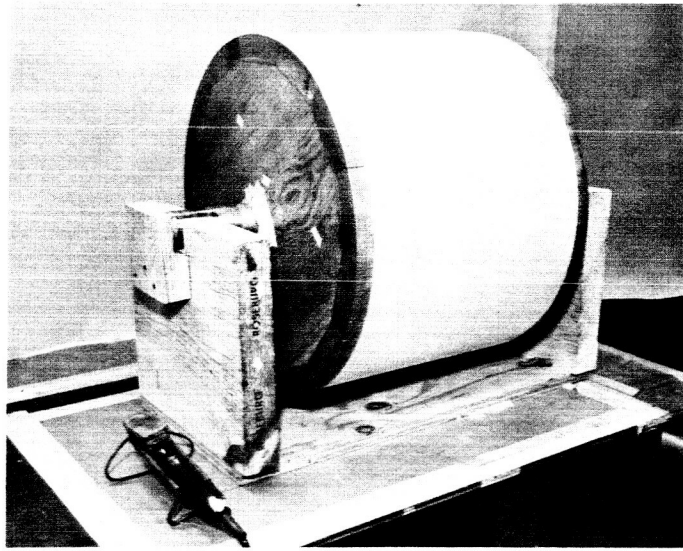
Figure 22. - Fabricated cylindrical drum for rf tests.
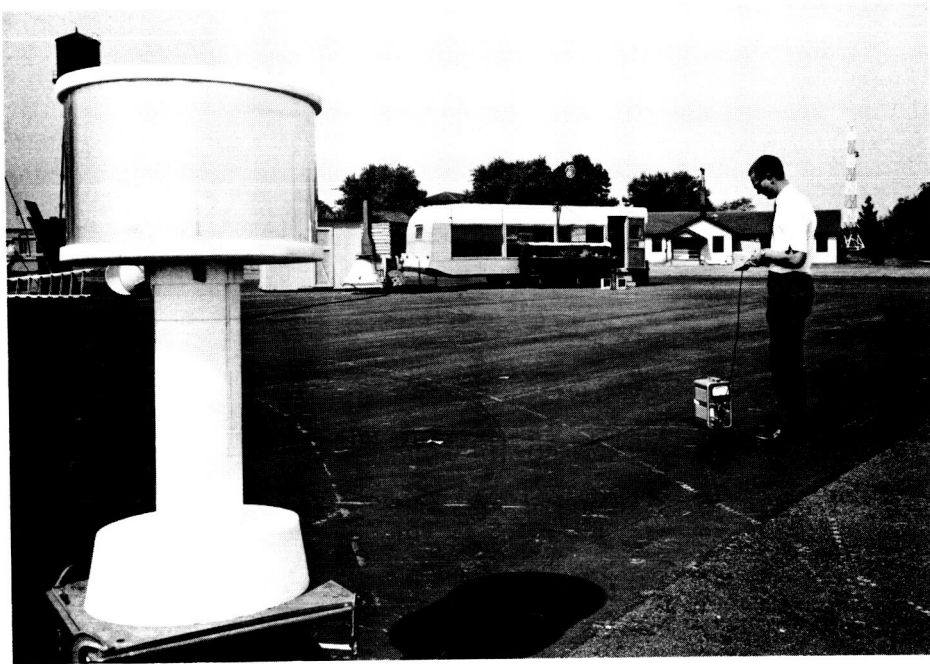
Figure 23. - Seam study test range.
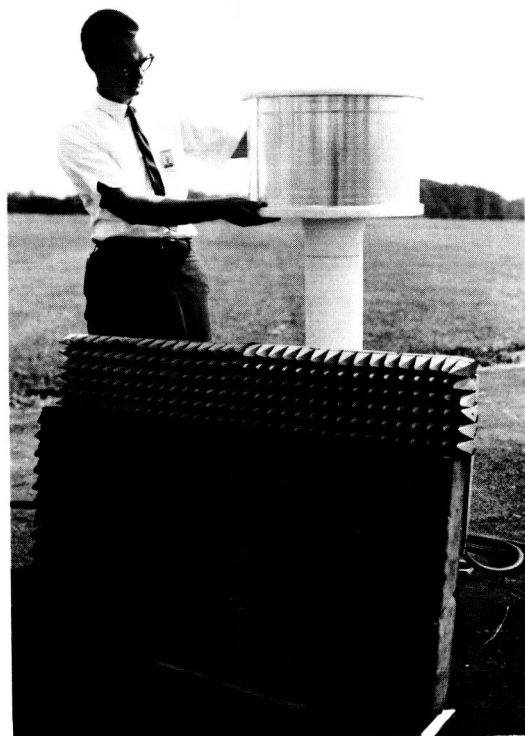
Figure 24. - Cylinder support column.

Figure 25. - Test results on seams using aluminum foil.
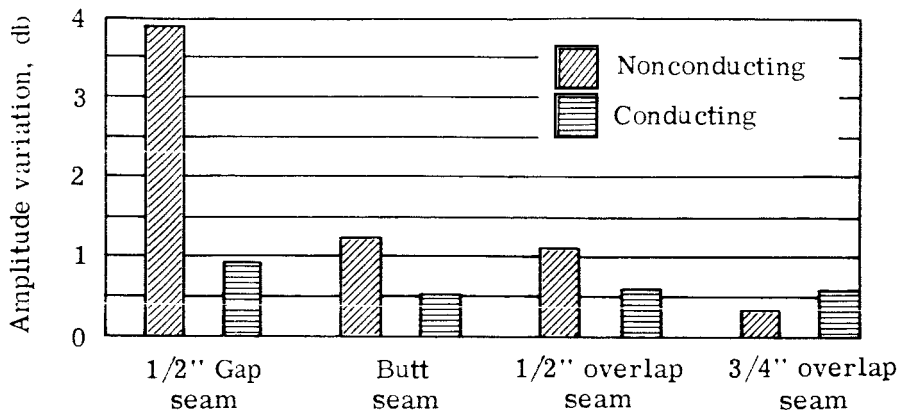
Figure 26. - Test results on seams using 80 x 80 copper wire mesh - parallel and perpendicular to polarization.
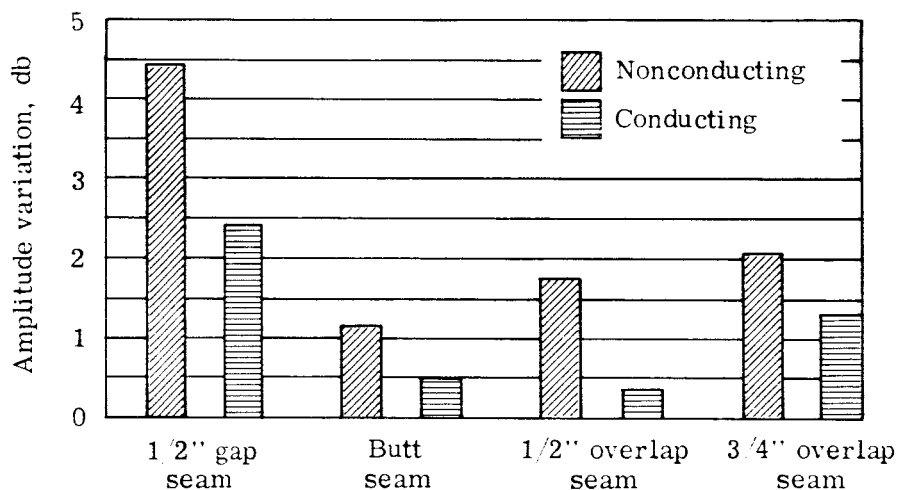
Figure 27. - Test results on seams using 80 x 80 copper wire mesh - 45° to polarization.

45
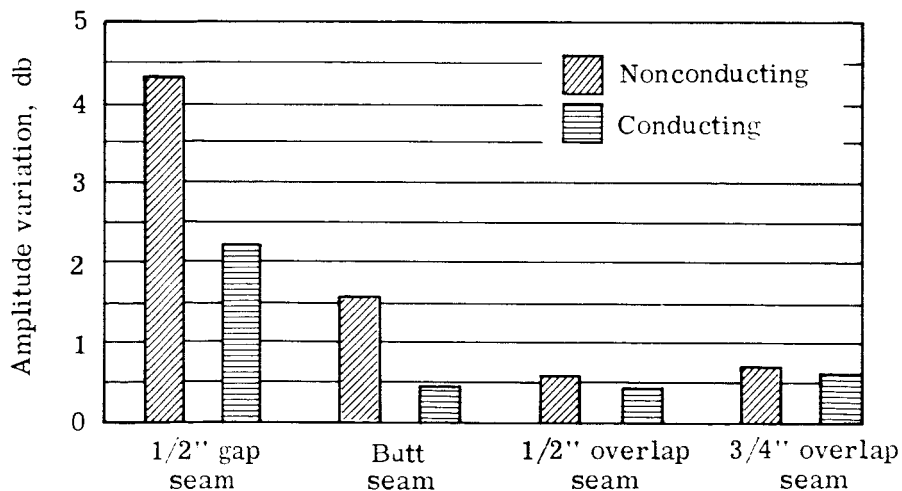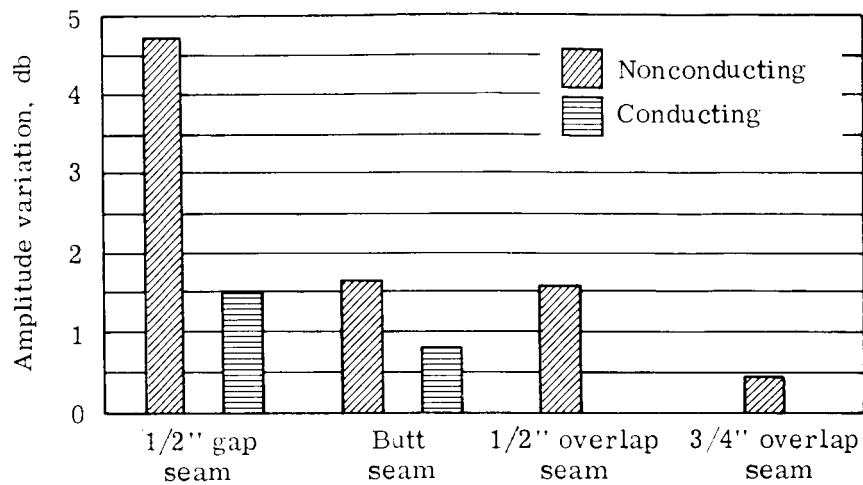
Figure 28. - Test results on seams using lenticular film grid material -
parallel and perpendicular to polarization.
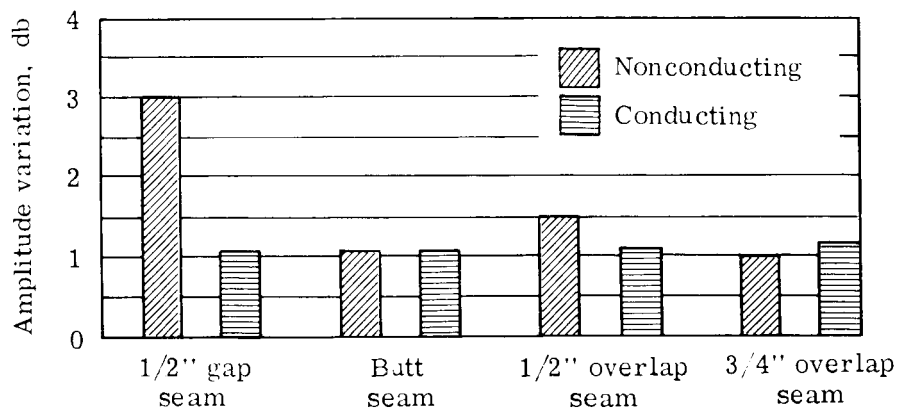
Figure 29. - Test results on seams using lenticular film grid material -
45° to polarization.

Typical mesh pattern
1.6-mil phosphor bronze wire - 24 x 24
0.7-mil photolyzable film; wt = 0.008 lb/ft^2

6" diam cap

Model "A"
Polar gore pattern

8 equal-spaced gores
0.75"-lap conductive seams

Model "A"

23"
(ref.)

Foam
2 lb/cu ft

10.7

10.7

Model "B"

15" (typ)

Typical mesh pattern
1.6-mil phosphor bronze wire - 24 x 24
0.7-mil photolyzable film; wt = 0.008 lb/ft^2
0.75"-lap conductive seams

Wt   18 pounds (each half)
Diam = 60 inches
Circ = 188.496 inches
Arc length = 65.33 inches
Included angle = 78°
Radius   48.0 inches
Area (one side) = 23 ft^2

Model "B"
Equatorial gore pattern

Figure 30. – Five-foot diameter lenticular models.

47
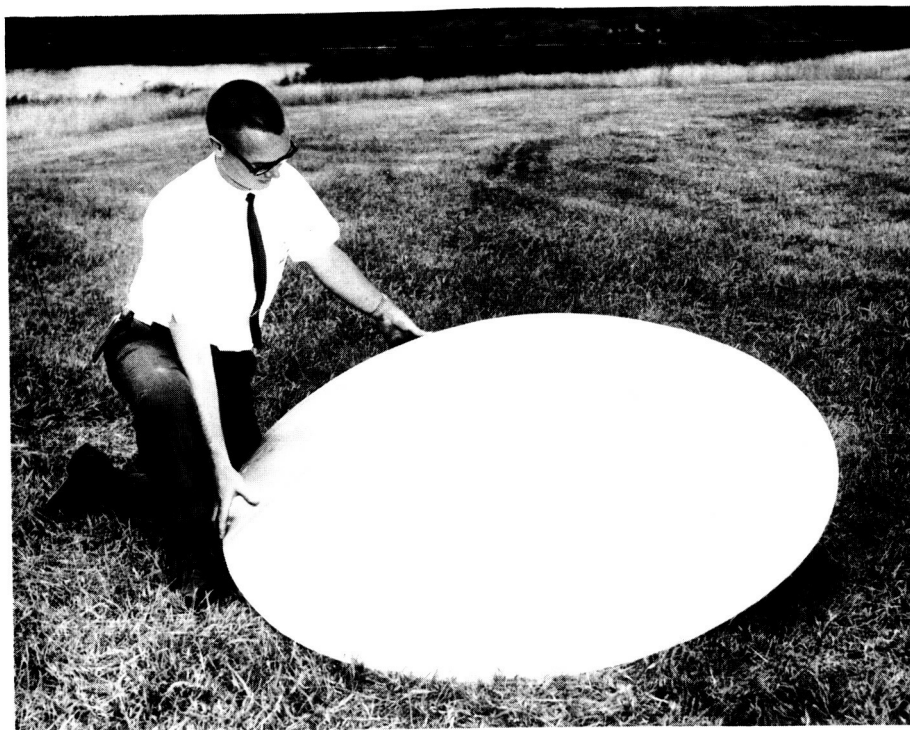
Model A - Polar gore pattern
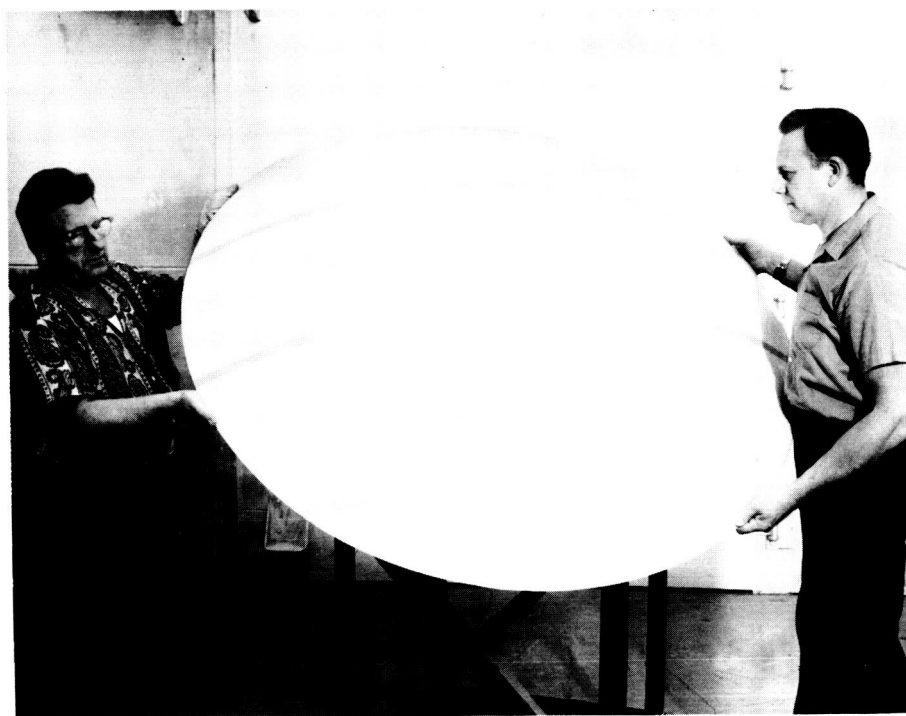
Model B - Equatorial gore pattern

Figure 31. - Simulated inflatable models covered with lenticular grid material.
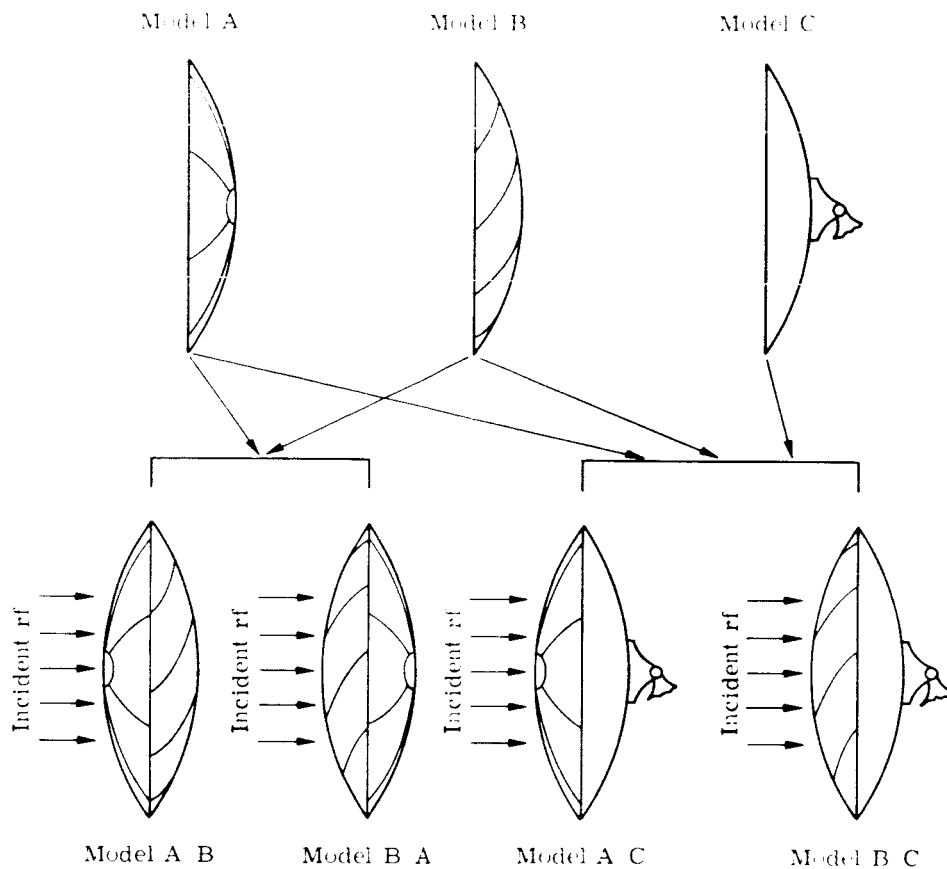
Figure 32. - Test models - Phase III.
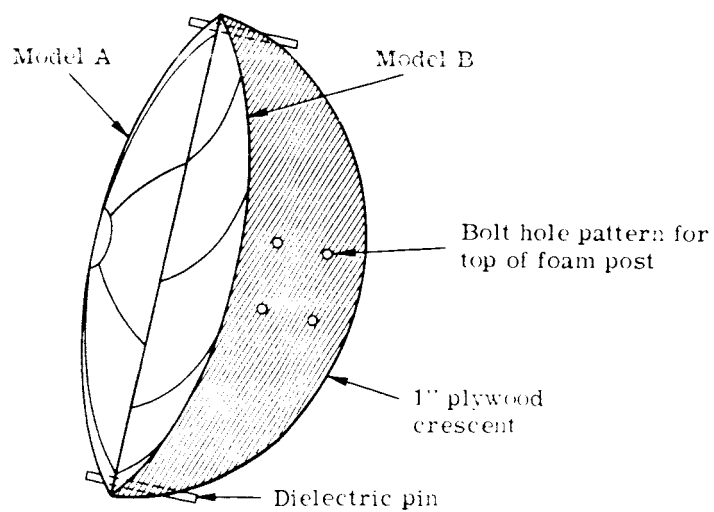
Figure 33. - Mounting scheme for
A/B and B/A tests - Phase III.
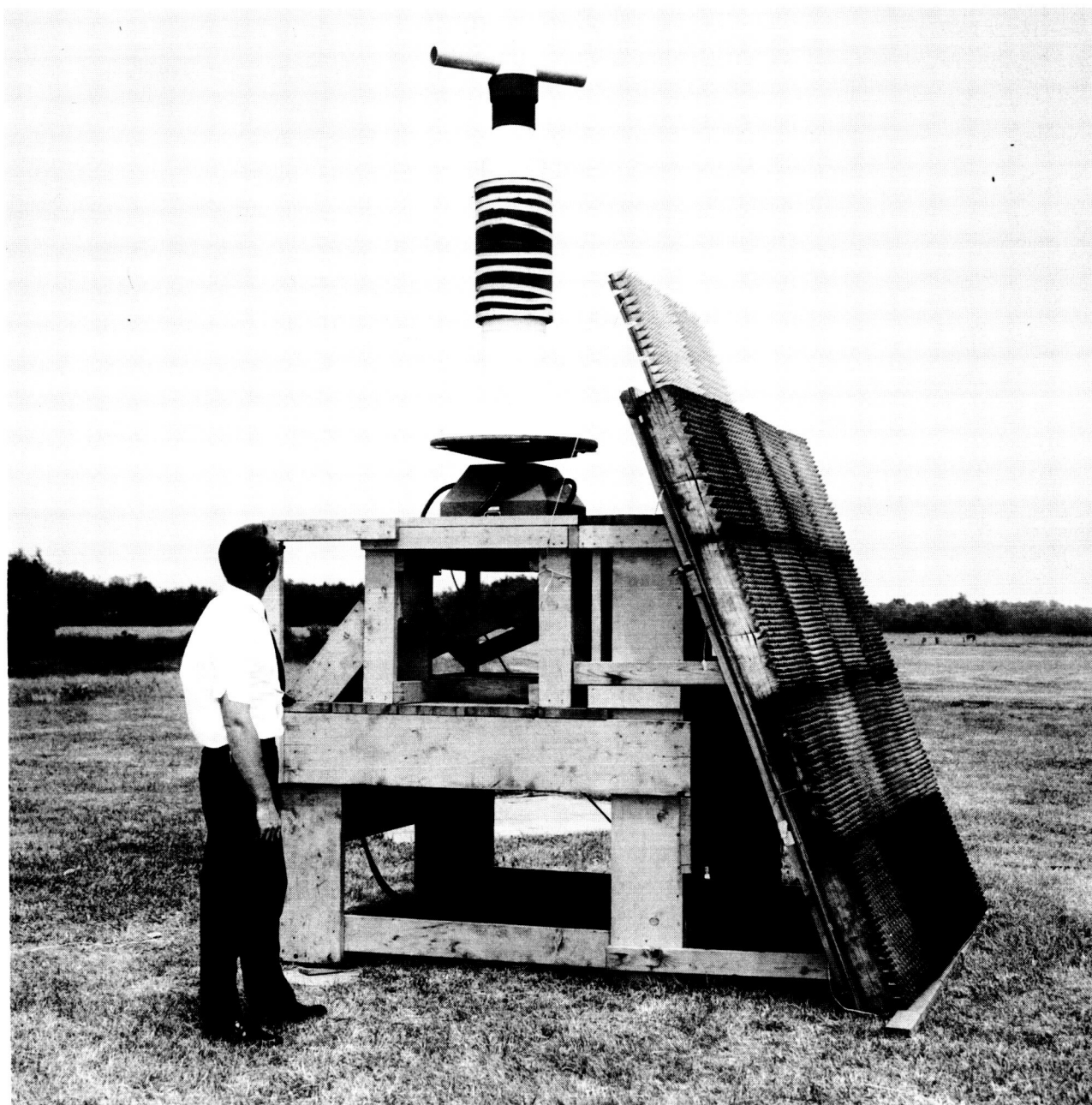
Figure 34. - Reference cylinder on mount.
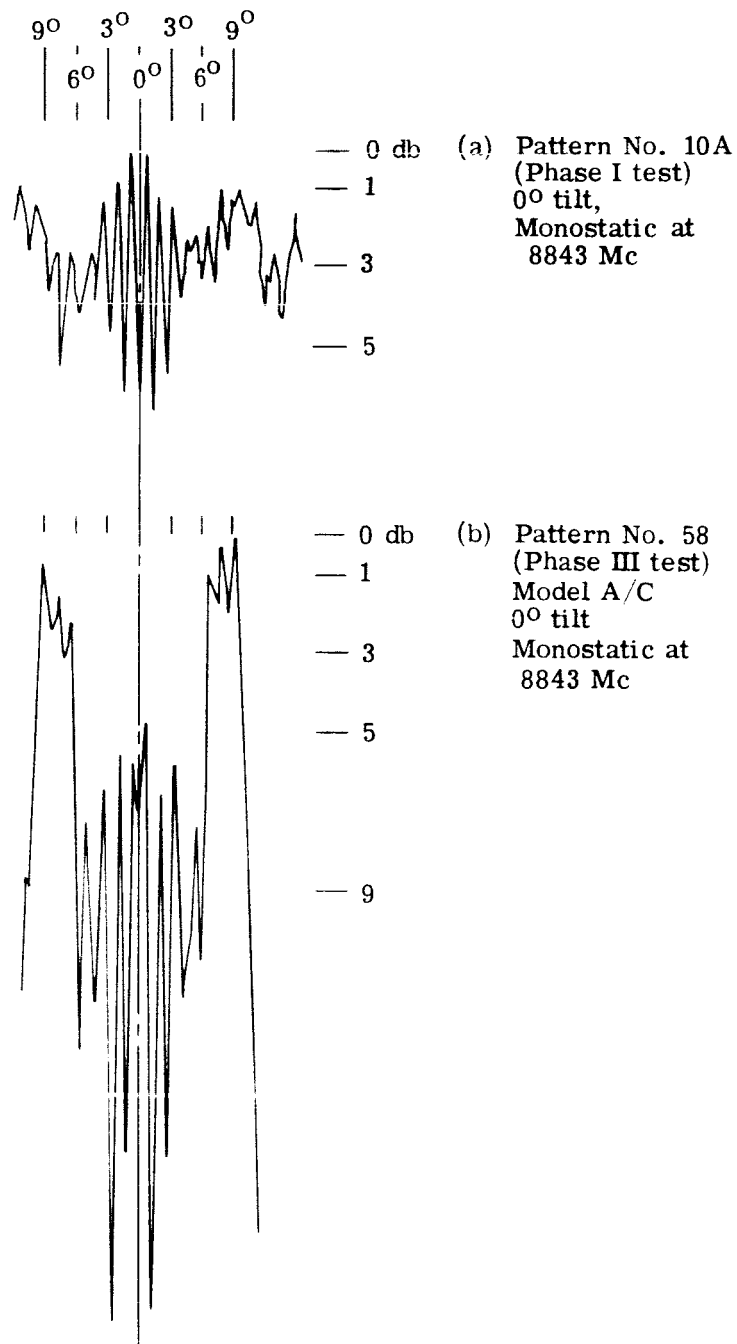
Figure 35. - Return from Phase I Model and Model A/C showing scintillation structure at the center of response.
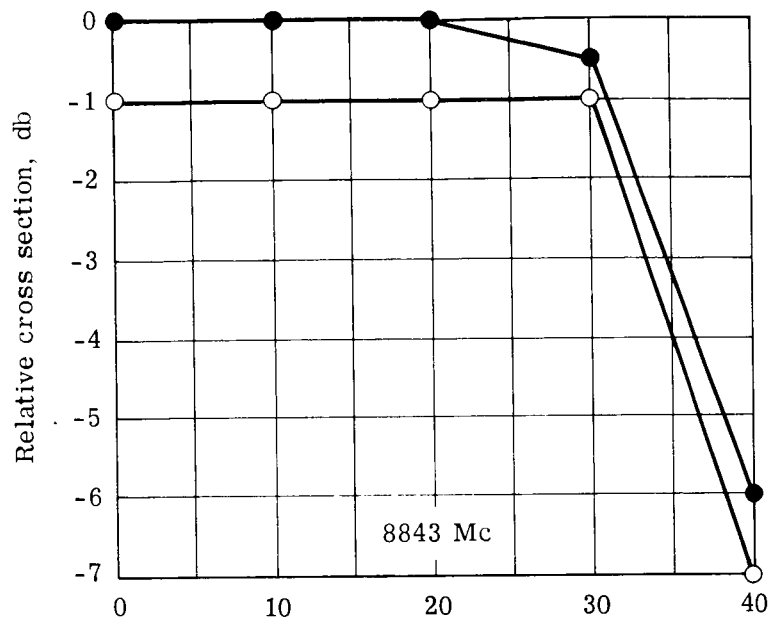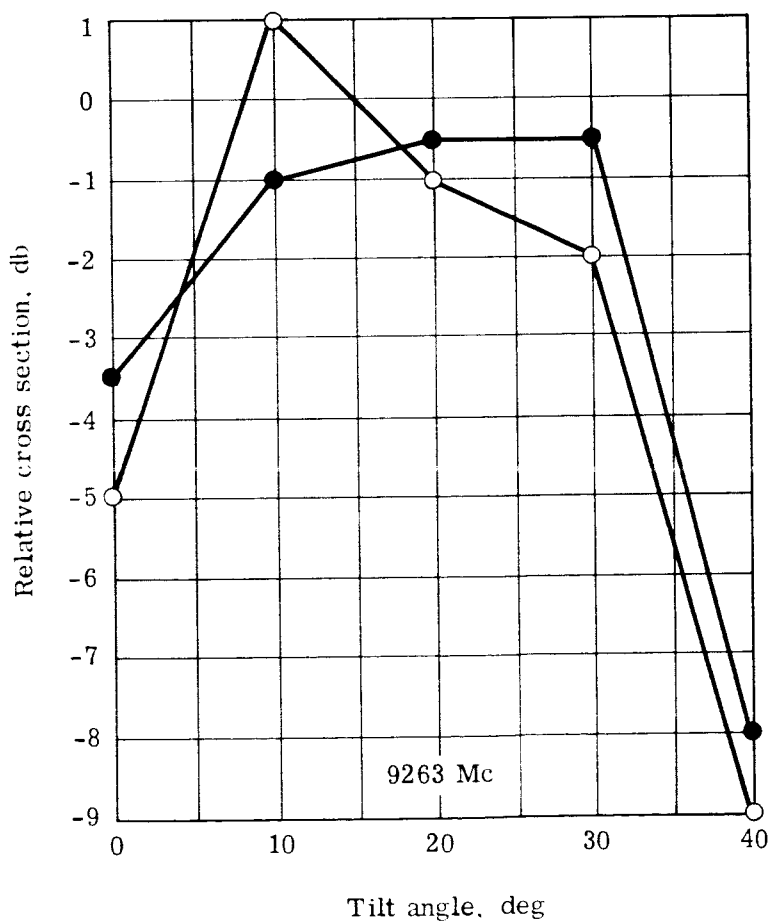
Figure 36. - Relative mean radar cross sections for Phase I Model without booms.
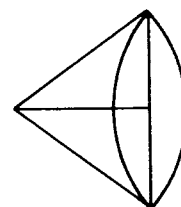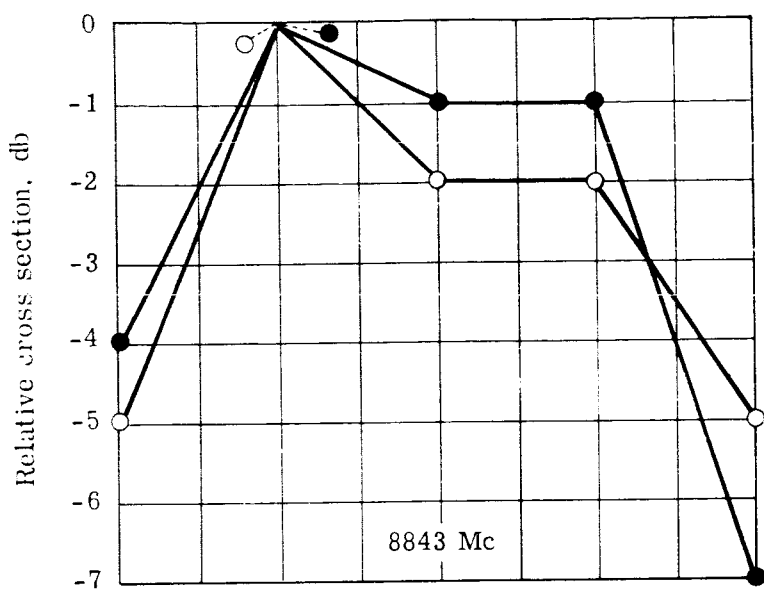
Figure 37. – Relative mean radar cross sections for Phase I Model with booms.
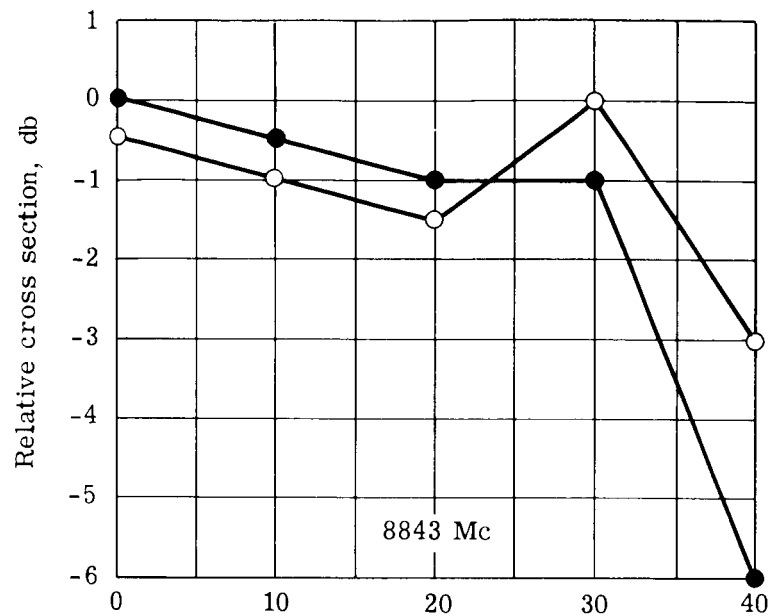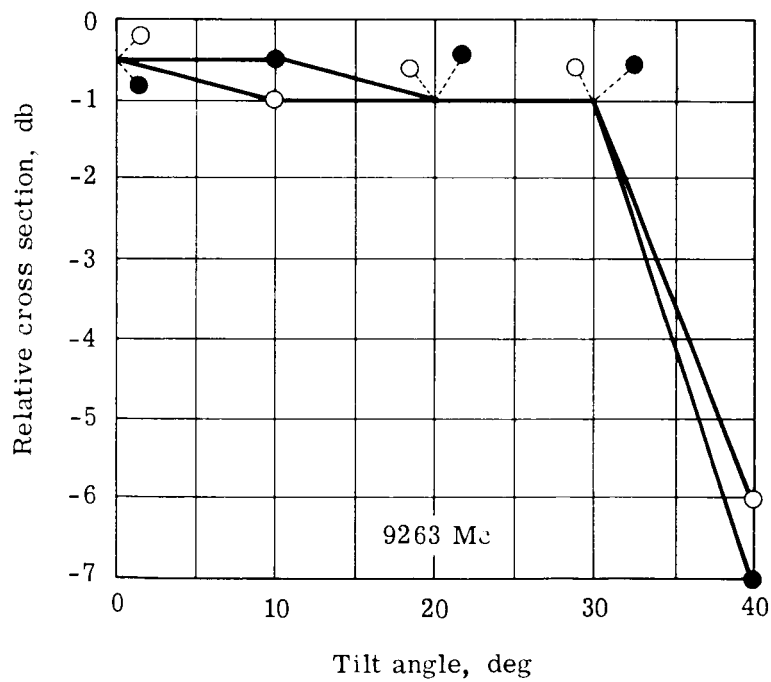
Figure 38. - Relative mean radar cross sections for Phase III Model A/C.
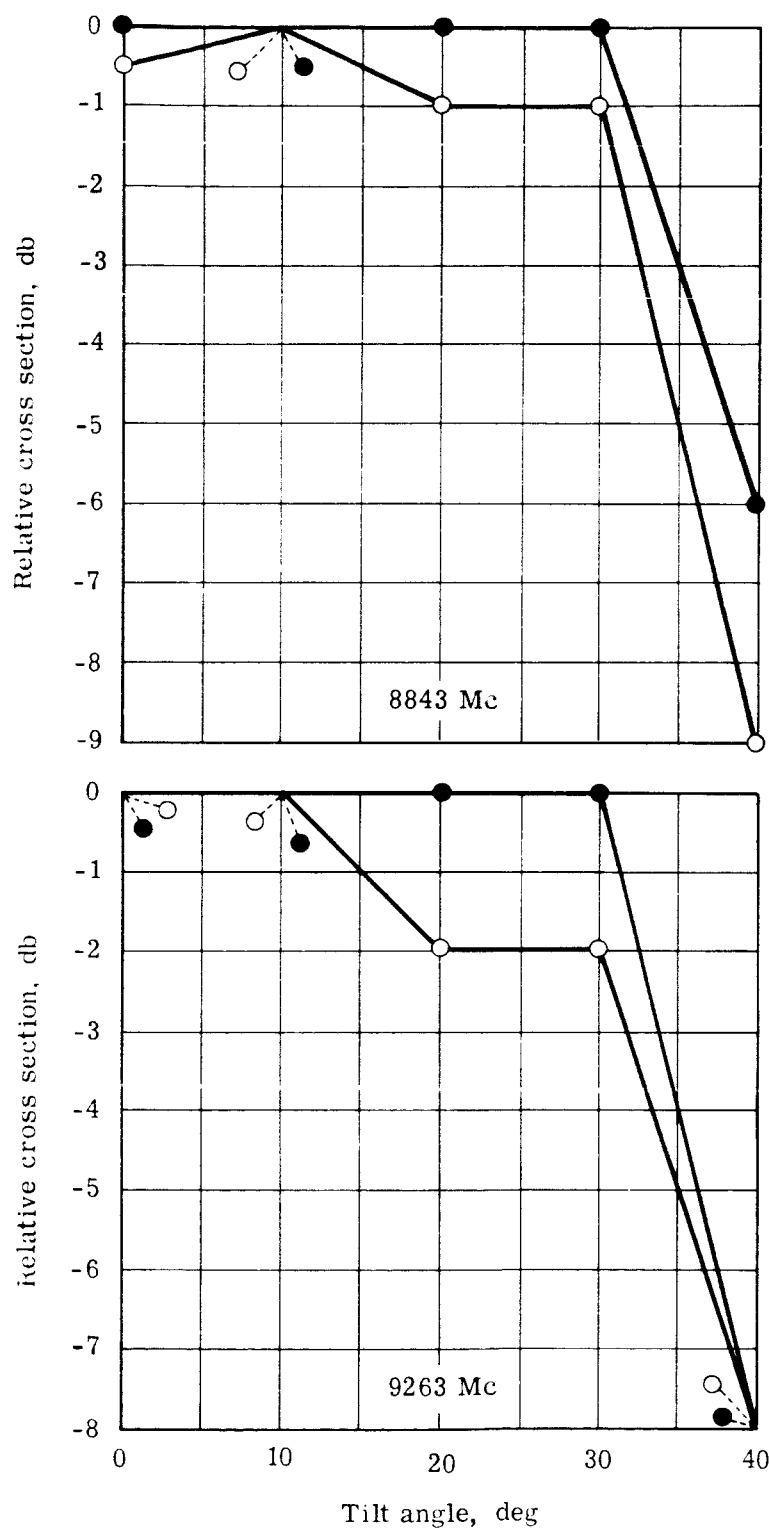
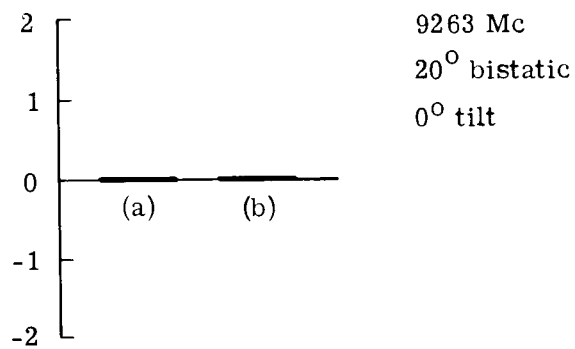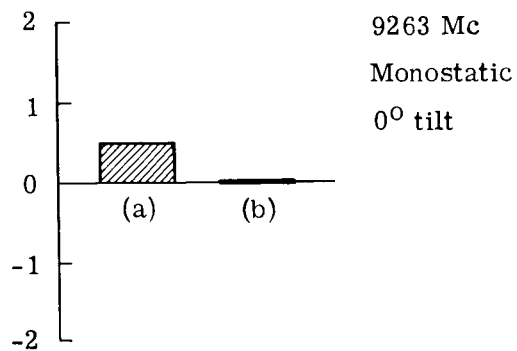Figure 39. – Relative mean radar cross sections for Phase III Model B/C.

55
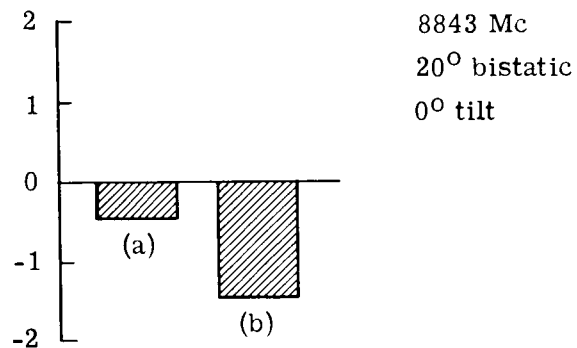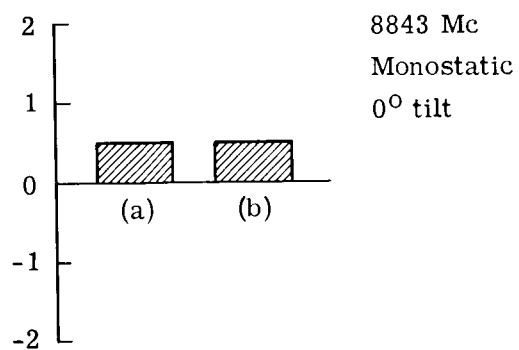
Figure 40. - Relative mean radar cross sections for Phase III Models A/B and B/A.

REFERENCES

1. Anon.: Feasibility Study and Preliminary Design of Gravity Gradient Stabilized Lenticular Test Satellite. GER 11502, Goodyear Aerospace Corp, June 1964.

2. Smith, A.G.: Notes on the Analysis, Prediction, and Experimental Verification of the Monostatic Radar Cross-Section Characteristics of a Passive Communications Satellite of Lenticular Configuration. Technical Memorandum, Research Triangle Institute, 6 October 1964.

3. Stratton: Electromagnetic Theory. McGraw-Hill Book Company, New York, 1941, pp 563-570.

4. Mentzer, J.R.: Scattering and Diffraction of Radio Waves. Pergamon Press, New York, 1955.

5. Jasik, H., ed.: Antenna Engineering Handbook. McGraw-Hill Book Company, New York, 1961.

6. Anon.: Study, Fabrication, and Testing of Passive Satellite Models, Grid-Sphere Type. Report SEG TDR 64-52, August 1964. (Contract AF 33(657)-11537, Goodyear Aerospace Corp, Akron, Ohio. Report GER 11568).

7. Stahler, Ylo E.: The Echo Area of Partially Transparent Spheres (The Grid-Sphere Effect). 1965 National Conference Proceedings of the 17th Annual National Aerospace Electronics Conference, pp 205-212.

8. Anon.: Echo II Experimental Program Final Report. Rep. 523-0556818-001D3N (Contract NAS 5-3640), Collins Radio Company, 15 July 1965.

9. Andreasen, M.G.: Back-Scattering Cross Section of a Thin Dielectric Spherical Shell. IRE Transactions on Antennas and Propagation, Vol. AP-5, Number 3, July 1957, pp. 267-270.

10. Andreasen, M.G.: Radiation from a Radial Dipole Through a Thin Dielectric Spherical Shell. IRE Transactions on Antennas and Propagation, Vol. AP-5, Oct. 1957, pp. 337-342.

11. Richmond, J.H.: Scattering by Thin, Spherical, Reactive Shell. Appendix A of Reference 6, pp. 74-79.